Available online at www.sciencedirect.com
ScienceDirect
International Journal of Thermal Sciences 48 (2009) 50–72
International Journal of Thermal Sciences
www.elsevier.com/locate/ijts

Magnetothermoelastic analysis of multilayered conical shells subjected to magnetic and vapor fields

Z.Y. Lee *

Department of Mechanical Engineering, Hsiuping Institute of Technology, No. 11 Gungye Road, Dali City, Taichung 412, Taiwan, ROC

Received 6 September 2007; received in revised form 28 January 2008; accepted 7 February 2008

Available online 14 March 2008

Abstract

This paper considers problems of the three-dimensional axisymmetric quasi-static coupled magnetothermoelasticity for the laminated circular conical shells subjected to magnetic and vapor fields. The water vapor temperature and pressure relation are assumed for the inner boundary. The water vapor temperature and pressure data were obtained from a thermodynamic steam table. The formulation begins with the basic equations of magnetothermoelasticity in curvilinear circular conical coordinates. Laplace transform and finite difference methods are used to analyze problems. The solution is obtained by using the matrix similarity transformation and inverse Laplace transform. We obtain solutions for the temperature and thermal deformation distributions in a transient and steady state. Moreover, the computational procedures established in this thesis, can solve the generalized magnetothermoelasticity problem for multilayered conical shells with nonhomogeneous materials.

Keywords: Magnetothermoelastic; Conical multilayered; Laplace transform

1. Introduction

The increased interest recently in magnetothermoelasticity can be attributed to the increased study of magnetothermomechanical coupled behavior in smart structures. The interaction between magnetic, thermal and mechanical fields in a hollow cylinder is usually encountered in space shuttles, supersonic airplanes, rockets and missiles, plasma physics and the corresponding measurement techniques of magnetothermoelasticity. The interaction between the magnetic, thermal and mechanical fields in a hollow cylinder gives rise to the transient coupled theory of magnetothermoelasticity. This theory is applicable to analyze a wide range of magnetically, thermally and mechanically coupled phenomena in the mixed state.

There are relatively very few studies on quasi-static coupled thermoelasticity for laminated conical shells under various mechanical loads, although there have been many studies on the structure of thin conical shells. Al-Huniti and Al-Nimr [1] presented the transient thermoelastic response of a thin composite plate composed of a dominant matrix and an insert is investigated. The plate is heated by exposing the matrix to a heating source in the form of a step function. The hyperbolic heat conduction model is used to determine the thermal behavior of the plate, which is assumed to be lumped in the transverse direction. The dominant temperature of the matrix is used to evaluate the thermal stresses. Hosseini-Tehrani and Hosseini-Godarzi [2] presented a boundary element method using Laplace transform in time domain is developed for the analysis of fracture mechanics considering transient coupled thermoelasticity problems with relaxation time in two-dimensional finite domain. The dynamic thermoelastic model of Lord and Shulman are selected for showing finite thermal propagation speed. The Laplace transform method is applied to the time domain and the resulting equations in the transformed field are discretized using boundary element method. Actual physical quantities in time domain is obtained, using the numerical inversion of the Laplace transform method. Ram et al. [3] presented a general solution to the field equations of generalized thermodiffusion in an elastic solid has been obtained, in the transformed form, using the Fourier transform. Assuming the disturbances to be harmonically time dependent, the transformed solution is obtained in the frequency domain. Wang et al. [4,5] presented an analyt-

* Tel.: +886 4 24961123, ext 1103; fax: +886 4 24961108.
E-mail address: zylee@mail.hit.edu.tw.

1290-0729/$ – see front matter
doi:10.1016/j.ijthermalsci.2008.02.002

Nomenclature

Θ, T	dimensional and nondimensional temperature
σ_η^*, σ_θ^*, σ_ς^*	dimensional normal stress
σ_x, σ_θ, σ_z	the nondimensional normal stresses
$\tau_{\eta\theta}^*$, $\tau_{\eta\zeta}^*$, $\tau_{\theta\zeta}^*$	dimensional shear stress
ε_η^*, ε_θ^*, ε_ζ^*	dimensional normal strain
$\gamma_{\eta\theta}^*$, $\gamma_{\eta\varsigma}^*$, $\gamma_{\theta\varsigma}^*$	dimensional shear strain
$\nu_{\eta\zeta}$, $\nu_{\eta\theta}$, $\nu_{\theta\zeta}$	Poisson's ratio
α_η, α_θ, α_ζ	linear thermal expansion coefficients
E_η, E_θ, E_ζ	Young's modulus
$G_{\eta\theta}$, $G_{\eta\zeta}$, $G_{\theta\zeta}$	shear modulus.
k_η, k_ζ	the thermal conductivities
τ	the dimensional time
x	nondimensional meridional direction
z	nondimensional normal direction
u_x, u_z	nondimensional displacement components
τ_{xz}	nondimensional shear stress
λ	Lame's constant
ρ	density
C_v	specific heat
Θ_0	reference temperature
L	z-direction length
μ	magnetic permeability
H_0	initial constant magnetic field vector

ical method for stress wave propagation of spherically symmetric motion in laminated piezoelectric shells subjected to thermal shock and electric excitation loads. The analytical expressions of displacement, stresses and electric potential for each spherically symmetric shell layer are obtained by means of finite Hankel transforms and Laplace transforms. Wang et al. [6–8] presented a theoretical method for analyzing magnetothermoelastic responses and perturbation of the magnetic field vector in a conducting orthotropic and non-homogeneous thermoelastic cylinder subjected to thermal shock. By making use of finite Hankle integral transforms the analytical expressions for magnetothermodynamic stress and perturbation response of an axial magnetic field vector in the orthotropic and non-homogeneous cylinder are obtained. Jianpong and Harik [9] presented an iterative finite difference method to determine the stresses and displacements from bending of axisymmetric conical shells. This method can be applied to short and long conical shells having simply supported, clamped, or free edges, and it can easily be extended to tapered conical shells and other types of axisymmetric shells. Based on thick shell theory, Lu, Mao and Winfield [10] discussed the stress distribution of thick laminated conical tubes under general loading. The effect of transverse shear is taken into account by a first-order theory. Governing equations are solved by a semi-analytical method that is a combination of Fourier series expansion, finite difference scheme and Riccati transfer matrix method. The method can be applied to the analysis of any axisymmetric laminated tube or shell that may approximately be divided into a series of conical shell segments. Based on the three-dimensional equations, Wu and Chiu [11] analyzed the thermal dynamic instability of laminated conical shells subjected to static and periodic thermal loads. By using the differential quadrature method and Bolotin's method, the boundary frequencies of the principal instability regions of cross-ply conical shell with simply supported boundary conditions can be obtained. Based on the governing equations of three-dimensional elasticity, an asymptotic theory was presented by Wu and Chiu [12] for the thermoelastic buckling analysis of laminated composite conical shells subjected to a uniform temperature change. The perturbation method is used to determine the critical thermal loads. Performing a straightforward derivation, the asymptotic formulation leads to recursive sets of governing equations for various orders. The critical thermal loads of simply supported, cross-ply conical shells have been studied to demonstrate the performance of the asymptotic theory.

Chen et al. [13,14] presented a new numerical technique-hybrid numerical method for the problem of a transient linear heat conduction system. They applied the Laplace transform to remove the time-dependence from the governing equations and boundary conditions, and solved the transformed equations with the finite element and finite difference method. Finally, the transformed temperature was inverted by numerical inversion of the Laplace transform. It was demonstrated that the method can accurately determine stable solutions at a specific time. Jane and Lee [15] considered the same problem by using the Laplace transform and the finite difference method. In this case, the cylinder was composed of multiple layers of different materials, and there was no limit to the number of annular layers of the cylinder in the computational procedures. The Laplace transform and finite difference methods were used to analyze problems. They solutions were obtained for the temperature and thermal stress distributions in a transient state.

However, there have been few studies on the quasi-static coupled magnetothermoelasticity of laminated conical shells, due to difficulties in the theoretical analysis and the complexity of the mathematics. In this paper, we consider the three-dimensional quasi-static coupled magnetothermoelastic problems of multilayered conical shell with magnetic and vapor fields. The medium is without heat generation. Laplace transform and finite difference methods are used, which are quite effective and powerful to obtain solutions of a wide range of transient thermal stress problems as previously shown [16,17].

2. Formulation

Consider the laminated circular conical shell composed of multiple layers with different materials. The material of each region is elastic and axisymmetric. Moreover, it is assumed that perfect contact is maintained at the interface between two adjacent layers and there is assumed to be a different thickness h_i of

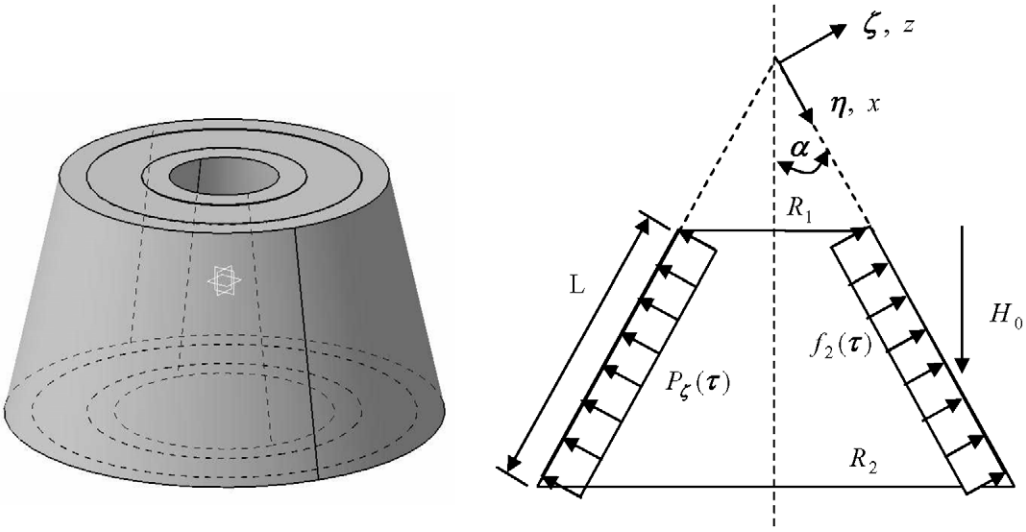

Fig. 1. Physical model and system coordinates for the circular conical shell.

each layer. For the laminated circular conical shell subjected to magnetic and vapor fields is presented. A set of the orthogonal curvilinear coordinates (η, θ, ζ) is located on the internal surface, as shown in Fig. 1, in which η is the meridional direction, θ is the circumferential direction, and ζ is the normal direction; Let R_1 and R_2 be the radii of the cone at the small and large edges, respectively, α be the semi-vertex angle of the cone, L be the cone length along the generator and $R = R(\eta, \zeta)$ be the variable radius of the circular conical shell at any point along the η-direction. Furthermore, the outer and inner temperatures are assumed to be f_1 and f_2, respectively. The temperatures at both ends are assumed to be f_3 and f_4, respectively.

The constitutive relations including the thermal effect for the kth layer of the conical shell are given by

$$\begin{Bmatrix} \sigma_\eta^* \\ \sigma_\theta^* \\ \sigma_\zeta^* \\ \tau_{\eta\theta}^* \\ \tau_{\eta\zeta}^* \\ \tau_{\theta\zeta}^* \end{Bmatrix} = \begin{bmatrix} C_{11} & C_{12} & C_{13} & 0 & 0 & 0 \\ C_{12} & C_{22} & C_{23} & 0 & 0 & 0 \\ C_{13} & C_{23} & C_{33} & 0 & 0 & 0 \\ 0 & 0 & 0 & C_{44} & 0 & 0 \\ 0 & 0 & 0 & 0 & C_{55} & 0 \\ 0 & 0 & 0 & 0 & 0 & C_{66} \end{bmatrix} \times \begin{Bmatrix} \varepsilon_\eta^* - \alpha_\eta \overline{\Theta} \\ \varepsilon_\theta^* - \alpha_\theta \overline{\Theta} \\ \varepsilon_\zeta^* - \alpha_\zeta \overline{\Theta} \\ \gamma_{\eta\theta}^* \\ \gamma_{\eta\zeta}^* \\ \gamma_{\theta\zeta}^* \end{Bmatrix} \tag{1}$$

in which $\overline{\Theta} = \Theta - \Theta_0$, and

$$C_{11} = (1/A)\big[E_\eta(1 - \nu_{\theta\zeta}\nu_{\zeta\theta})\big]$$
$$C_{12} = (1/A)\big[E_\theta(\nu_{\zeta\theta} + \nu_{\zeta\theta}\nu_{\eta\zeta})\big]$$
$$C_{13} = (1/A)\big[E_\zeta(\nu_{\eta\zeta} + \nu_{\eta\theta}\nu_{\theta\zeta})\big]$$
$$C_{22} = (1/A)\big[E_\theta(1 - \nu_{\eta\zeta}\nu_{\zeta\eta})\big]$$
$$C_{23} = (1/A)\big[E_\zeta(\nu_{\theta\zeta} + \nu_{\theta\eta}\nu_{\eta\zeta})\big]$$
$$C_{33} = (1/A)\big[E_\zeta(1 - \nu_{\eta\theta}\nu_{\theta\eta})\big]$$
$$A = 1 - \nu_{\eta\theta}\nu_{\theta\eta} - \nu_{\theta\zeta}\nu_{\zeta\theta} - 2\nu_{\theta\eta}\nu_{\zeta\theta}\nu_{\eta\zeta}$$
$$C_{44} = G_{\eta\theta}, \qquad C_{55} = G_{\eta\zeta}, \qquad C_{66} = G_{\theta\zeta}$$

where C_{ij} are the stiffness coefficients. Eq. (1) represents the constitutive equations for an orthotropic material where the number of independent elastic material coefficients is nine.

The kinematics relations for the kth layer of the conical shell can be expressed as

$$\begin{Bmatrix} \varepsilon_\eta^* \\ \varepsilon_\theta^* \\ \varepsilon_\zeta^* \\ \gamma_{\eta\theta}^* \\ \gamma_{\eta\zeta}^* \\ \gamma_{\theta\zeta}^* \end{Bmatrix} = \begin{bmatrix} \frac{\partial}{\partial\eta} & 0 & 0 \\ \frac{\sin\alpha}{R} & 0 & \frac{\cos\alpha}{R} \\ 0 & 0 & \frac{\partial}{\partial\zeta} \\ 0 & \frac{\partial}{\partial\eta} - \frac{\sin\alpha}{R} & 0 \\ \frac{\partial}{\partial\zeta} & 0 & \frac{\partial}{\partial\eta} \\ 0 & \frac{\partial}{\partial\zeta} - \frac{\cos\alpha}{R} & 0 \end{bmatrix} \begin{Bmatrix} U_\eta \\ U_\theta \\ U_\zeta \end{Bmatrix} \tag{2}$$

where R is given by $R(\eta, \zeta) = R_1 + \eta\sin\alpha + \zeta\cos\alpha$ for the circular conical shell; U_η, U_θ and U_ζ are dimensional displacement components along η-, θ- and ζ-direction, respectively.

Consider a long, circular conical shell with perfect conductivity placed initially magnetic field $\vec{H}_0$, as shown in Fig. 1. Let this conical shell be subjected to a rapid change in temperature $T(\zeta, t)$ produced by the absorption of an electromagnetic pulse or γ-ray pulse radiant energy. There will then be an interaction between deformation of the conical shell and perturbation of the magnetic field vector in the circular conical shell. Assuming that the magnetic permeability, μ, of the conical shell equals the magnetic permeability of the medium around it and omitting displacement electric currents, the governing electrodynamic Maxwell equations [18] for a perfectly conducting, elastic body are given by

$$\vec{J} = \mathrm{Curl}\,\vec{h}, \qquad -\mu\frac{\partial\vec{h}}{\partial t} = \mathrm{Curl}\,\vec{e}$$
$$\mathrm{div}\,\vec{h} = 0, \qquad \vec{e} = -\mu\left(\frac{\partial\vec{U}}{\partial t} \times \vec{H}_0\right) \tag{3}$$

Applying an initial magnetic field vector $\vec{H}_0$ in cylindrical polar coordinates $(\eta, \theta, \zeta)$to Eq. (3) we have

$$\vec{U} = \big(0, 0, u(\zeta, t)\big), \qquad \vec{e} = \mu\left(0, H_0\frac{\partial u}{\partial t}, 0\right) \tag{4a}$$

$$\vec{h} = (h_\eta, 0, 0), \qquad \vec{J} = \left(0, \frac{\partial h_\eta}{\partial \zeta}, 0\right) \tag{4b}$$

$$h_\eta = -H_0\left(\frac{\partial u}{\partial \zeta}\right) \tag{4c}$$

From Eqs. (3) and (4), the magnetoelastic equation of the conical shell becomes

$$\cos\alpha\cdot\sigma_\zeta^* + R\frac{\partial\sigma_\zeta^*}{\partial\zeta} + \sin\alpha\cdot\tau_{\zeta\eta}^* + R\frac{\partial\tau_{\zeta\eta}^*}{\partial\eta} - \cos\alpha\cdot\sigma_\theta^* + f_\zeta = 0 \tag{5}$$

where f_ζ is defined as Lorentz's force, which may be written as

$$f_\zeta = R\mu H_0^2\frac{\partial U_\zeta^2}{\partial\zeta^2}$$

The equation of equilibrium for a circular conical shell along the η- and ζ-direction, respectively, can be written as

$$\sin\alpha\cdot\sigma_\eta^* + R\frac{\partial\sigma_\eta^*}{\partial\eta} + \cos\alpha\cdot\tau_{\eta\zeta}^* + R\frac{\partial\tau_{\eta\varsigma}^*}{\partial\varsigma} - \sin\alpha\cdot\sigma_\theta^* = 0 \tag{6}$$

$$\cos\alpha\cdot\sigma_\zeta^* + R\frac{\partial\sigma_\zeta^*}{\partial\zeta} + \sin\alpha\cdot\tau_{\zeta\eta}^* + R\frac{\partial\tau_{\zeta\eta}^*}{\partial\eta} - \cos\alpha\cdot\sigma_\theta^* + R\mu H_0^2\frac{\partial^2 U_\zeta}{\partial\zeta^2} = 0 \tag{7}$$

The coupled transient heat conduction equation for the kth layer of the conical shell can be written as

$$k_\eta\frac{\partial^2\overline{\Theta}}{\partial\eta^2} + k_\eta\frac{\sin\alpha}{R}\frac{\partial\overline{\Theta}}{\partial\eta} + k_\zeta\frac{\partial^2\overline{\Theta}}{\partial\zeta^2} + k_\zeta\frac{\cos\alpha}{R}\frac{\partial\overline{\Theta}}{\partial\zeta} = \rho C_v\frac{\partial\overline{\Theta}}{\partial\tau} + \Theta_0\beta_\eta\frac{\partial\varepsilon_\eta^*}{\partial\tau} + \Theta_0\beta_\theta\frac{\partial\varepsilon_\theta^*}{\partial\tau} + \Theta_0\beta_\zeta\frac{\partial\varepsilon_\zeta^*}{\partial\tau} \tag{8}$$

in which

$$\beta_\eta = (1/A)\big[E_\eta(1-\nu_{\theta\zeta}\nu_{\zeta\theta})\alpha_\eta + E_\theta(\nu_{\eta\theta}+\nu_{\zeta\theta}\nu_{\eta\zeta})\alpha_\theta + E_\zeta(\nu_{\eta\zeta}+\nu_{\eta\theta}\nu_{\theta\zeta})\alpha_\zeta\big]$$

$$\beta_\theta = (1/A)\big[E_\theta(\nu_{\eta\theta}+\nu_{\zeta\theta}\nu_{\eta\zeta})\alpha_\eta + E_\theta(1-\nu_{\eta\zeta}\nu_{\zeta\eta})\alpha_\theta + E_\zeta(\nu_{\theta\zeta}+\nu_{\theta\eta}\nu_{\eta\zeta})\alpha_\zeta\big]$$

$$\beta_\zeta = (1/A)\big[E_\zeta(\nu_{\eta\zeta}+\nu_{\eta\theta}\nu_{\theta\zeta})\alpha_\eta + E_\zeta(\nu_{\theta\zeta}+\nu_{\theta\eta}\nu_{\eta\zeta})\alpha_\theta + E_\zeta(1-\nu_{\eta\theta}\nu_{\theta\eta})\alpha_\zeta\big]$$

Substitution of Eq. (2) into Eq. (1) yields the stress-displacement relations for the kth layer as

$$\sigma_{\nu k}^* = C_{11}\frac{\partial U_\eta}{\partial\eta} + C_{12}\frac{\sin\alpha}{R}U_\eta + C_{12}\frac{\cos\alpha}{R}U_\zeta + C_{13}\frac{\partial U_\zeta}{\partial\zeta} - \beta_\eta\overline{\Theta} \tag{9}$$

$$\sigma_{\theta k}^* = C_{12}\frac{\partial U_\eta}{\partial\eta} + C_{22}\frac{\sin\alpha}{R}U_\eta + C_{22}\frac{\cos\alpha}{R}U_\zeta + C_{23}\frac{\partial U_\zeta}{\partial\zeta} - \beta_\theta\overline{\Theta} \tag{10}$$

$$\sigma_{\zeta k}^* = C_{13}\frac{\partial U_\eta}{\partial\eta} + C_{23}\frac{\sin\alpha}{R}U_\eta + C_{23}\frac{\cos\alpha}{R}U_\zeta + C_{33}\frac{\partial U_\zeta}{\partial\zeta} - \beta_\zeta\overline{\Theta} \tag{11}$$

$$\tau_{\eta\zeta k}^* = C_{55}\left(\frac{\partial U_\zeta}{\partial\eta} + \frac{\partial U_\eta}{\partial\zeta}\right) \tag{12}$$

where $\sigma_{\eta k}^*$, $\sigma_{\theta k}^*$ and $\sigma_{\zeta k}^*$ are the dimensional normal stresses for the kth layer, and $\tau_{\eta\zeta k}^*$ is the dimensional shear stress for the kth layer.

By substituting Eqs. (9)–(12) into Eqs. (6)–(7), the equation of equilibrium for a circular conical shell along the η- and ζ-direction, respectively, can be rewritten as

$$\begin{aligned} &C_{11}\frac{\partial^2 U_\eta}{\partial\eta^2} + C_{11}\frac{\sin\alpha}{R}\frac{\partial U_\eta}{\partial\eta} - C_{22}\frac{\sin^2\alpha}{R^2}U_\eta + C_{55}\frac{\partial^2 U_\eta}{\partial\zeta^2} \\ &+ C_{55}\frac{\cos\alpha}{R}\frac{\partial U_\eta}{\partial\zeta} + (C_{13}+C_{55})\frac{\partial^2 U_\zeta}{\partial\eta\partial\zeta} \\ &+ (C_{13}-C_{23})\frac{\sin\alpha}{R}\frac{\partial U_\zeta}{\partial\zeta} + (C_{12}+C_{55})\frac{\cos\alpha}{R}\frac{\partial U_\zeta}{\partial\eta} \\ &- C_{22}\frac{\sin\alpha\cos\alpha}{R^2}U_\zeta - \beta_\eta\frac{\partial\overline{\Theta}}{\partial\eta} - (\beta_\eta-\beta_\theta)\frac{\sin\alpha}{R}\overline{\Theta} = 0 \end{aligned} \tag{13}$$

$$\begin{aligned} &C_{33}\frac{\partial^2 U_\zeta}{\partial\zeta^2} + C_{33}\frac{\cos\alpha}{R}\frac{\partial U_\zeta}{\partial\zeta} - C_{22}\frac{\cos^2\alpha}{R^2}U_\zeta + C_{55}\frac{\partial^2 U_\zeta}{\partial\eta^2} \\ &+ C_{55}\frac{\sin\alpha}{R}\frac{\partial U_\zeta}{\partial\eta} + (C_{13}+C_{55})\frac{\partial^2 U_\eta}{\partial\eta\partial\zeta} \\ &+ (C_{13}-C_{12})\frac{\cos\alpha}{R}\frac{\partial U_\eta}{\partial\eta} + (C_{23}+C_{55})\frac{\sin\alpha}{R}\frac{\partial U_\eta}{\partial\zeta} \\ &- C_{22}\frac{\sin\alpha\cos\alpha}{R^2}U_\eta - \beta_\zeta\frac{\partial\overline{\Theta}}{\partial\zeta} - (\beta_\zeta-\beta_\theta)\frac{\cos\alpha}{R}\overline{\Theta} \\ &+ \mu H_0^2\frac{\partial^2 U_\zeta}{\partial\zeta^2} = 0 \end{aligned} \tag{14}$$

By substituting Eq. (2) into Eq. (8), the coupled transient heat conduction equation for the kth layer of the conical shell also can be rewritten as

$$\begin{aligned} &k_\eta\frac{\partial^2\overline{\Theta}}{\partial\eta^2} + k_\eta\frac{\sin\alpha}{R}\frac{\partial\overline{\Theta}}{\partial\eta} + k_\zeta\frac{\partial^2\overline{\Theta}}{\partial\zeta^2} + k_\zeta\frac{\cos\alpha}{R}\frac{\partial\overline{\Theta}}{\partial\zeta} \\ &= \rho C_v\frac{\partial\overline{\Theta}}{\partial\tau} + \Theta_0\beta_\eta\frac{\partial}{\partial\eta}\left(\frac{\partial U_\eta}{\partial\tau}\right) + \Theta_0\beta_\theta\frac{\sin\alpha}{R}\frac{\partial U_\eta}{\partial\tau} \\ &+ \Theta_0\beta_\theta\frac{\cos\alpha}{R}\frac{\partial U_\zeta}{\partial\tau} + \Theta_0\beta_\zeta\frac{\partial}{\partial\zeta}\left(\frac{\partial U_\zeta}{\partial\tau}\right) \end{aligned} \tag{15}$$

In this study, let the boundary surfaces of the laminated circular conical shells remain traction-free and subjected to the heating process. The boundary conditions at the outer and top boundary surfaces can be expressed as

$$\sigma_\zeta^*(\eta,\zeta,\tau) = 0, \qquad \Theta_1 = \Theta_0 + f_1 \quad \text{at } \zeta = (R_2 - R_1)/\cos\alpha$$
$$\sigma_\eta^*(\eta,\zeta,\tau) = 0, \qquad \Theta_3 = \Theta_0 + f_3 \quad \text{at } \eta = R_1/\sin\alpha$$

Let the boundary surfaces of the laminated circular conical shells remain at time-dependent boundary temperature and subjected to a dynamic pressure. It is assumed that the dynamic

pressure $P(\tau)$ depends on time in the normal direction, thus the boundary conditions at the inner and bottom boundary surfaces can be considered as

$$\sigma^*_\zeta(\eta,\zeta,\tau)=P(\tau), \qquad \Theta_2=\Theta_0+f_2 \quad \text{at } \zeta=R_1/\cos\alpha$$
$$\sigma^*_\eta(\eta,\zeta,\tau)=0, \qquad \Theta_4=\Theta_0+f_4 \quad \text{at } \eta=L+R_1/\sin\alpha$$

At the interface between the kth and $(k+1)$th layers, assuming perfect contact, the interface conditions are

$$\left(U_\eta, U_\zeta, \sigma^*_\zeta, \tau^*_{\eta\zeta}, q, \overline{\Theta}\right)_k = \left(U_\eta, U_\zeta, \sigma^*_\zeta, \tau^*_{\eta\zeta}, q, \overline{\Theta}\right)_{k+1}$$

where q is the heat flux per unit area per unit time.

The initial condition is $U_\eta = U_\zeta = \dot{U}_\eta = \dot{U}_\zeta = \overline{\Theta} = \dot{\overline{\Theta}} = 0$ at $\tau = 0$.

The nondimensional variables for the circular multi-layered conical shells are defined as follows:

$$x=\eta(\sin\alpha/R_1), \qquad z=\zeta(\cos\alpha/R_1)$$
$$T(\Theta-\Theta_0)/\Theta_0=\overline{\Theta}/\Theta_0, \qquad u_x=U_\eta\left(\frac{\beta_\eta}{\rho C_v}\right)_k\Big/\left(\frac{R_1}{\sin\alpha}\right)$$
$$u_z=U_\zeta\left(\frac{\beta_\eta}{\rho C_v}\right)_k\Big/\left(\frac{R_1}{\cos\alpha}\right), \qquad t=\tau\left(\frac{k_\eta}{\rho C_v}\right)_1\Big/\left(\frac{R_1}{\sin\alpha}\right)^2$$
$$a_{1k}=a_{2k}=\left(\frac{k_\eta}{\rho C_v}\right)_k\Big/\left(\frac{k_\eta}{\rho C_v}\right)_1$$
$$a_{3k}=a_{4k}=\left(\frac{k_\zeta}{\rho C_v}\right)_k\Big/\left(\frac{k_\eta}{\rho C_v}\right)_1$$
$$a_{5k}=a_{6k}=\left(\frac{\beta_\theta}{\rho C_v}\right)_k\Big/\left(\frac{\beta_\eta}{\rho C_v}\right)_k$$
$$a_{7k}=\left(\frac{\beta_\zeta}{\rho C_v}\right)_k\Big/\left(\frac{\beta_\eta}{\rho C_v}\right)_k$$
$$b_{1k}=b_{5k}=C_{22}/C_{11}, \qquad b_{2k}=b_{3k}=C_{55}\left(\frac{\cos\alpha}{\sin\alpha}\right)^2/C_{11}$$
$$b_{4k}=(C_{13}-C_{23})/C_{11}, \qquad b_{6k}=(C_{12}+C_{55})/C_{11}$$
$$b_{7k}=(C_{13}+C_{55})/C_{11}, \qquad b_{8k}=\Theta_0\beta_\eta\left(\frac{\beta_\eta}{\rho C_v}\right)_k/C_{11}$$
$$b_{9k}=\Theta_0(\beta_\eta-\beta_\theta)\left(\frac{\beta_\eta}{\rho C_v}\right)_k/C_{11}$$
$$c_{1k}=c_{5k}=C_{22}\left(\frac{\cos\alpha}{\sin\alpha}\right)^2/C_{55}$$
$$c_{2k}=\left(C_{33}+\mu H_0^2\right)\left(\frac{\cos\alpha}{\sin\alpha}\right)^2/C_{55}$$
$$c_{3k}=C_{33}\left(\frac{\cos\alpha}{\sin\alpha}\right)^2/C_{55}$$
$$c_{4k}=(C_{23}+C_{55})\left(\frac{\cos\alpha}{\sin\alpha}\right)^2/C_{55}$$
$$c_{6k}=(C_{13}-C_{12})\left(\frac{\cos\alpha}{\sin\alpha}\right)^2/C_{55}$$
$$c_{7k}=(C_{13}+C_{55})\left(\frac{\cos\alpha}{\sin\alpha}\right)^2/C_{55}$$
$$c_{8k}=\Theta_0\beta_\zeta\left(\frac{\beta_\eta}{\rho C_v}\right)_k\left(\frac{\cos\alpha}{\sin\alpha}\right)^2/C_{55}$$
$$c_{9k}=\Theta_0(\beta_\zeta-\beta_\theta)\left(\frac{\beta_\eta}{\rho C_v}\right)_k\left(\frac{\cos\alpha}{\sin\alpha}\right)^2/C_{55}$$
$${}_1Q_k=C_{11}/\left[\beta_{\eta1}\left(\frac{\beta_\eta}{\rho C_v}\right)_k\Theta_0\right]$$
$${}_2Q_k=C_{12}/\left[\beta_{\eta1}\left(\frac{\beta_\eta}{\rho C_v}\right)_k\Theta_0\right]$$
$${}_3Q_k=C_{13}/\left[\beta_{\eta1}\left(\frac{\beta_\eta}{\rho C_v}\right)_k\Theta_0\right]$$
$${}_4Q_k=\beta_{\eta k}/\beta_{\eta1}, \qquad {}_1R_k=C_{12}/\left[\beta_{\theta1}\left(\frac{\beta_\eta}{\rho C_v}\right)_k\Theta_0\right]$$
$${}_2R_k=C_{22}/\left[\beta_{\theta1}\left(\frac{\beta_\eta}{\rho C_v}\right)_k\Theta_0\right]$$
$${}_3R_k=C_{23}/\left[\beta_{\theta1}\left(\frac{\beta_\eta}{\rho C_v}\right)_k\Theta_0\right]$$
$${}_4R_k=\beta_{\theta k}/\beta_{\theta1}, \qquad {}_1P_k=C_{13}/\left[\beta_{\zeta1}\left(\frac{\beta_\eta}{\rho C_v}\right)_k\Theta_0\right]$$
$${}_2P_k=C_{23}/\left[\beta_{\zeta1}\left(\frac{\beta_\eta}{\rho C_v}\right)_k\Theta_0\right]$$
$${}_3P_k=C_{33}/\left[\beta_{\zeta1}\left(\frac{\beta_\eta}{\rho C_v}\right)_k\Theta_0\right]$$
$${}_4P_k=\beta_{\zeta k}/\beta_{\zeta1}, \qquad \sigma_{xk}=\sigma^*_{\eta k}/(\beta_{\eta1}\Theta_0)$$
$$\sigma_{\theta k}=\sigma^*_{\theta k}/(\beta_{\theta1}\Theta_0), \qquad \sigma_{zk}=\sigma^*_{\zeta k}/(\beta_{\zeta1}\Theta_0)$$
$$\sigma_{\theta k}=\sigma^*_{\theta k}/(\beta_{\theta1}\Theta_0), \qquad \tau_{xz}=\tau^*_{\eta\zeta}/C_{551}$$
$${}_1S_k=\left(\frac{C_{55}}{C_{551}}\right)\left(\frac{\cos\alpha}{\sin\alpha}\right)\Big/\left(\frac{\beta_\eta}{\rho C_v}\right)_k$$
$${}_2S_k=\left(\frac{C_{55}}{C_{551}}\right)\left(\frac{\sin\alpha}{\cos\alpha}\right)\Big/\left(\frac{\beta_\eta}{\rho C_v}\right)_k$$

3. Computational procedures

By applying the transformation of coordinates, the variable radius $R(\eta,\zeta)$ of the circular conical shell can be rewritten as $r=r(x,z)=1+x+z$.

By substituting the nondimensional quantities into the governing equations (13), (14) and (15), and constitutive relations (9) to (12), we obtain the following nondimensional equations:

$$\frac{\partial^2 u_x}{\partial x^2}+\frac{1}{r}\frac{\partial u_x}{\partial x}-\frac{b_{1k}}{r^2}u_x+b_{2k}\frac{\partial^2 u_x}{\partial z^2}+\frac{b_{3k}}{r^2}\frac{\partial u_x}{\partial z}+\frac{b_{4k}}{r^2}\frac{\partial u_z}{\partial z}-\frac{b_{5k}}{r^2}u_z+\frac{b_{6k}}{r^2}\frac{\partial u_z}{\partial x}++b_{7k}\frac{\partial^2 u_z}{\partial x\partial z}-b_{8k}\frac{\partial T}{\partial x}-\frac{c_{9k}}{r}T=0 \tag{16}$$

$$\frac{\partial^2 u_z}{\partial x^2}+\frac{1}{r}\frac{\partial u_z}{\partial x}-\frac{c_{1k}}{r^2}u_z+c_{2k}\frac{\partial^2 u_z}{\partial z^2}+\frac{c_{3k}}{r}\frac{\partial u_z}{\partial z}+\frac{c_{4k}}{r}\frac{\partial u_x}{\partial z}-\frac{c_{5k}}{r^2}u_x+\frac{c_{6k}}{r}\frac{\partial u_x}{\partial x}+c_{7k}\frac{\partial^2 u_x}{\partial x\partial z}-c_{8k}\frac{\partial T}{\partial z}-\frac{c_{9k}}{r}T=0 \tag{17}$$

$$\left\{a_{1k}\frac{\partial^2}{\partial x^2}+\frac{a_{2k}}{r}\frac{\partial}{\partial x}+a_{3k}\frac{\partial^2}{\partial z^2}+\frac{a_{4k}}{r}\frac{\partial}{\partial z}\right\}T = \frac{\partial T}{\partial t}+\frac{\partial}{\partial x}\left(\frac{\partial u_x}{\partial t}\right)+\frac{a_{5k}}{r}\left(\frac{\partial u_x}{\partial t}\right) + \frac{a_{6k}}{r}\left(\frac{\partial u_z}{\partial t}\right)+a_{7k}\frac{\partial}{\partial z}\left(\frac{\partial u_z}{\partial t}\right) \tag{18}$$

$$\sigma_{xk} = {}_1Q_k\frac{\partial u_x}{\partial x}+{}_2Q_k\frac{u_x}{r}+{}_2Q_k\frac{u_x}{r}+{}_3Q_k\frac{\partial u_z}{\partial z}-{}_4Q_kT \tag{19}$$

$$\sigma_{\theta k} = {}_1R_k\frac{\partial u_x}{\partial x}+{}_2R_k\frac{u_x}{r}+{}_2R_k\frac{u_x}{r}+{}_3R_k\frac{\partial u_z}{\partial z}-{}_4R_kT \tag{20}$$

$$\sigma_{zk} = {}_1P_k\frac{\partial u_x}{\partial x}+{}_2P_k\frac{u_x}{r}+{}_2P_k\frac{u_x}{r}+{}_3P_k\frac{\partial u_z}{\partial z}-{}_4P_kT \tag{21}$$

$$\tau_{xzk} = {}_1S_k\frac{\partial u_x}{\partial z}+{}_2S_k\frac{\partial u_z}{\partial x} \tag{22}$$

The nondimensional boundary conditions can be expressed as

$$\begin{array}{lll}\sigma_z(x,z,t)=0, & T_1=f_1/\Theta_0 & \text{at } z=z_{\text{outer}}\\ \sigma_x(x,z,t)=0, & T_3=f_3/\Theta_0 & \text{at } x=x_{\text{top}}\\ \sigma_z(x,z,t)=P(t), & T_2=f_2(t)/\Theta_0 & \text{at } z=z_{\text{inner}}\\ \sigma_x(x,z,t)=0, & T_4=f_4/\Theta_0 & \text{at } x=x_{\text{bottom}}\end{array}$$

The nondimensional interface conditions between the kth and $(k+1)$th layers can be expressed as

$$(u_x,u_z,\sigma_z,\tau_{xz},q,T)_k=(u_x,u_z,\sigma_z,\tau_{xz},q,T)_{k+1}$$

By applying the central difference scheme in Eqs. (16)–(22), the following discretized equations are obtained as

$$\begin{aligned}&\frac{u_{xi+1,j}-2u_{xi,j}+u_{xi-1,j}}{(\Delta x)^2}+\frac{1}{r_{i,j}}\frac{u_{xi+1,j}-u_{xi-1,j}}{2\Delta x}\\ &-\frac{b_{1k}}{r_{i,j}^2}u_{xi,j}+b_{2k}\frac{u_{xi,j+1}-2u_{xi,j}+u_{xi,j-1}}{(\Delta z)^2}\\ &+\frac{b_{2k}}{r_{i,j}}\frac{u_{xi,j+1}-u_{xi,j-1}}{2\Delta z}+\frac{b_{3k}}{r_{i,j}}\frac{u_{zi,j+1}-u_{zi,j-1}}{2\Delta z}\\ &-\frac{b_{1k}}{r_{i,j}^2}u_{zi,j}+\frac{b_{4k}}{r_{i,j}}\frac{u_{zi+1,j}-u_{zi-1,j}}{2\Delta x}\\ &+b_{5k}\frac{u_{zi+1,j+1}-u_{zi+1,j-1}-u_{zi-1,j+1}+u_{zi-1,j-1}}{4\Delta x\Delta z}\\ &-b_{6k}\frac{T_{i+1,j}-T_{i-1,j}}{2\Delta x}-\frac{b_{7k}}{r_{i,j}}T_{i,j}=0\end{aligned} \tag{23}$$

$$\begin{aligned}&\frac{u_{zi+1,j}-2u_{zi,j}+u_{zi-1,j}}{(\Delta x)^2}+\frac{1}{r_{i,j}}\frac{u_{zi+1,j}-u_{zi-1,j}}{2\Delta x}-\frac{c_{1k}}{r_{i,j}^2}u_{zi,j}\\ &+c_{2k}\frac{u_{zi,j+1}-2u_{zi,j}+u_{zi,j-1}}{(\Delta z)^2}+\frac{c_{2k}}{r_{i,j}}\frac{u_{zi,j+1}-u_{zi,j-1}}{2\Delta z}\\ &+\frac{c_{3k}}{r_{i,j}}\frac{u_{xi,j+1}-u_{xi,j-1}}{2\Delta z}-\frac{c_{1k}}{r_{i,j}^2}u_{xi,j}\\ &+\frac{c_{4k}}{r_{i,j}}\frac{u_{xi+1,j}-u_{xi-1,j}}{2\Delta x}\\ &+c_{5k}\frac{u_{xi+1,j+1}-u_{xi+1,j-1}-u_{xi-1,j+1}+u_{xi-1,j-1}}{4\Delta x\Delta z}\\ &-c_{6k}\frac{T_{i,j+1}-T_{i,j-1}}{2\Delta z}-\frac{c_{7k}}{r_{i,j}}T_{i,j}=0\end{aligned} \tag{24}$$

$$\begin{aligned}&a_{1k}\frac{T_{i+1,j}-2T_{i,j}+T_{i-1,j}}{(\Delta x)^2}+a_{1k}\frac{1}{r_{i,j}}\frac{T_{i+1,j}-T_{i-1,j}}{2\Delta x}\\ &+a_{2k}\frac{T_{i,j+1}-2T_{i,j}+T_{i,j-1}}{(\Delta z)^2}+a_{2k}\frac{1}{r_{i,j}}\frac{T_{i,j+1}-T_{i,j-1}}{2\Delta z}\\ &=\frac{\partial T_{i,j}}{\partial t}+\frac{(\partial u_x/\partial t)_{i+1,j}-(\partial u_x/\partial t)_{i-1,j}}{2\Delta x}+\frac{a_{3k}}{r_{i,j}}\left(\frac{\partial u_x}{\partial t}\right)_{i,j}\\ &+\frac{a_{3k}}{r_{i,j}}\left(\frac{\partial u_z}{\partial t}\right)_{i,j}+a_{4k}\frac{(\partial u_z/\partial t)_{i,j+1}-(\partial u_z/\partial t)_{i,j-1}}{2\Delta z}\end{aligned} \tag{25}$$

$$\begin{aligned}\sigma_{xk} &= {}_1Q_k\frac{u_{xi+1,j}-u_{xi-1,j}}{2\Delta x}+{}_2Q_k\frac{u_{xi,j}}{r_{i,j}}+{}_2Q_k\frac{u_{zi,j}}{r_{i,j}}\\ &\quad+{}_3Q_k\frac{u_{zi,j+1}-u_{zi,j-1}}{2\Delta z}-{}_4Q_kT_{i,j}\end{aligned} \tag{26}$$

$$\begin{aligned}\sigma_{\theta k} &= {}_1R_k\frac{u_{xi+1,j}-u_{xi-1,j}}{2\Delta x}+{}_2R_k\frac{u_{xi,j}}{r_{i,j}}+{}_2R_k\frac{u_{zi,j}}{r_{i,j}}\\ &\quad+{}_3R_k\frac{u_{zi,j+1}-u_{zi,j-1}}{2\Delta z}-{}_4R_kT_{i,j}\end{aligned} \tag{27}$$

$$\begin{aligned}\sigma_{zk} &= {}_1P_k\frac{u_{xi+1,j}-u_{xi-1,j}}{2\Delta x}+{}_2P_k\frac{u_{xi,j}}{r_{i,j}}+{}_2P_k\frac{u_{zi,j}}{r_{i,j}}\\ &\quad+{}_3P_k\frac{u_{zi,j+1}-u_{zi,j-1}}{2\Delta z}-{}_4P_kT_{i,j}\end{aligned} \tag{28}$$

$$\tau_{xzk} = {}_1S_k\frac{u_{xi,j+1}-u_{xi,j-1}}{2\Delta z}+{}_2S_k\frac{u_{zi+1,j}-u_{zi-1,j}}{2\Delta x} \tag{29}$$

In order to remove the time derivatives from the governing equation and boundary conditions, the Laplace transform is used. The Laplace transform of a function $\Phi(t)$ and its inverse are defined by

$$\overline{\Phi}(s)=L\big[\Phi(t)\big]=\int_0^\infty e^{-st}\Phi(t)\,dt$$

$$\Phi(t)=L^{-1}\big[\overline{\Phi}(s)\big]=\frac{1}{2\pi i}\int_{c-i\infty}^{c+i\infty}e^{st}\overline{\Phi}(s)\,ds$$

By taking the Laplace transform for Eqs. (23)–(29), the following equations are obtained as

$$\begin{aligned}&\frac{\overline{u}_{xi+1,j}-2\overline{u}_{xi,j}+\overline{u}_{xi-1,j}}{(\Delta x)^2}+\frac{1}{r_{i,j}}\frac{\overline{u}_{xi+1,j}-\overline{u}_{xi-1,j}}{2\Delta x}\\ &-\frac{b_{1k}}{r_{i,j}^2}\overline{u}_{xi,j}+b_{2k}\frac{\overline{u}_{xi,j+1}-2\overline{u}_{xi,j}+\overline{u}_{xi,j-1}}{(\Delta z)^2}\\ &+\frac{b_{2k}}{r_{i,j}}\frac{\overline{u}_{xi,j+1}-\overline{u}_{xi,j-1}}{2\Delta z}+\frac{b_{3k}}{r_{i,j}}\frac{\overline{u}_{zi,j+1}-\overline{u}_{zi,j-1}}{2\Delta z}\\ &-\frac{b_{1k}}{r_{i,j}^2}\overline{u}_{zi,j}+\frac{b_{4k}}{r_{i,j}}\frac{\overline{u}_{zi+1,j}-\overline{u}_{zi-1,j}}{2\Delta x}\\ &+b_{5k}\frac{\overline{u}_{zi+1,j+1}-\overline{u}_{zi+1,j-1}-\overline{u}_{zi-1,j+1}+\overline{u}_{zi-1,j-1}}{4\Delta x\Delta z}\\ &-b_{6k}\frac{\overline{T}_{i+1,j}-\overline{T}_{i-1,j}}{2\Delta z}-\frac{b_{7k}}{r_{i,j}}\overline{T}_{i,j}=0\end{aligned} \tag{30}$$

$$\frac{\bar{u}_{zi+1,j}-2\bar{u}_{zi,j}+\bar{u}_{zi-1,j}}{(\Delta x)^2}+\frac{1}{r_{i,j}}\frac{\bar{u}_{zi+1,j}-\bar{u}_{zi-1,j}}{2\Delta x}-\frac{c_{1k}}{r_{i,j}^2}\bar{u}_{zi,j}+c_{2k}\frac{\bar{u}_{zi,j+1}-2\bar{u}_{zi,j}+\bar{u}_{zi,j-1}}{(\Delta z)^2}+\frac{c_{2k}}{r_{i,j}}\frac{\bar{u}_{zi,j+1}-\bar{u}_{zi,j-1}}{2\Delta z}+\frac{c_{3k}}{r_{i,j}}\frac{\bar{u}_{xi,j+1}-\bar{u}_{xi,j-1}}{2\Delta z}-\frac{c_{1k}}{r_{i,j}^2}\bar{u}_{xi,j}+\frac{c_{4k}}{r_{i,j}}\frac{\bar{u}_{xi+1,j}-\bar{u}_{xi-1,j}}{2\Delta x}+c_{5k}\frac{\bar{u}_{xi+1,j+1}-\bar{u}_{xi+1,j-1}-\bar{u}_{xi-1,j+1}+\bar{u}_{xi-1,j-1}}{4\Delta x\Delta z}-c_{6k}\frac{\overline{T}_{i,j+1}-\overline{T}_{i,j-1}}{2\Delta z}-\frac{c_{7k}}{r_{i,j}}\overline{T}_{i,j}=0 \tag{31}$$

$$a_{1k}\frac{\overline{T}_{i+1,j}-2\overline{T}_{i,j}+\overline{T}_{i-1,j}}{(\Delta x)^2}+a_{1k}\frac{1}{r_{i,j}}\frac{\overline{T}_{i+1,j}-\overline{T}_{i-1,j}}{2\Delta x}+a_{2k}\frac{\overline{T}_{i,j+1}-2\overline{T}_{i,j}+\overline{T}_{i,j-1}}{(\Delta z)^2}$$
$$a_{2k}\frac{1}{r_{i,j}}\frac{\overline{T}_{i,j+1}-\overline{T}_{i,j-1}}{2\Delta z}=(T_{i,j_{in}}+s\bar{T}_{i,j})+\frac{(u_{xin}+s\bar{u}_x)_{i+1,j}-(u_{xin}+s\bar{u}_x)_{i-1,j}}{2\Delta x}+\frac{a_{3k}}{r_{i,j}}(u_{xi,j_{in}}+s\bar{u}_{xi,j})+\frac{a_{3k}}{r_{i,j}}(u_{zi,j_{in}}+s\bar{u}_{zi,j})+a_{4k}\frac{(u_{zin}+s\bar{u}_z)_{i,j+1}-(u_{zin}+s\bar{u}_z)_{i,j-1}}{2\Delta z} \tag{32}$$

$$\bar{\sigma}_{xk}={}_1Q_k\frac{\bar{u}_{xi+1,j}-\bar{u}_{xi-1,j}}{2\Delta x}+{}_2Q_k\frac{\bar{u}_{xi,j}}{r_{i,j}}+{}_2Q_k\frac{\bar{u}_{zi,j}}{r_{i,j}}+{}_3Q_k\frac{\bar{u}_{zi,j+1}-\bar{u}_{zi,j-1}}{2\Delta z}-{}_4Q_k\overline{T}_{i,j} \tag{33}$$

$$\bar{\sigma}_{\theta k}={}_1R_k\frac{\bar{u}_{xi+1,j}-\bar{u}_{xi-1,j}}{2\Delta x}+{}_2R_k\frac{\bar{u}_{xi,j}}{r_{i,j}}+{}_2R_k\frac{\bar{u}_{zi,j}}{r_{i,j}}+{}_3R_k\frac{\bar{u}_{zi,j+1}-\bar{u}_{zi,j-1}}{2\Delta z}-{}_4R_k\overline{T}_{i,j} \tag{34}$$

$$\bar{\sigma}_{zk}={}_1P_k\frac{\bar{u}_{xi+1,j}-\bar{u}_{xi-1,j}}{2\Delta x}+{}_2P_k\frac{\bar{u}_{xi,j}}{r_{i,j}}+{}_2P_k\frac{\bar{u}_{zi,j}}{r_{i,j}}+{}_3P_k\frac{\bar{u}_{zi,j+1}-\bar{u}_{zi,j-1}}{2\Delta z}-{}_4P_k\overline{T}_{i,j} \tag{35}$$

$$\bar{\tau}_{xzk}={}_1S_k\frac{\bar{u}_{xi,j+1}-\bar{u}_{xi,j-1}}{2\Delta z}+{}_2S_k\frac{\bar{u}_{zi+1,j}-\bar{u}_{zi-1,j}}{2\Delta x} \tag{36}$$

After taking the Laplace transform, the boundary conditions in the transformed domain become

$$\sigma_z(x,z,t)=0,\qquad \overline{T}_1=\frac{\overline{f}_1}{\Theta_0}\quad \text{at } z=z_{\text{outer}}$$
$$\sigma_x(x,z,t)=0,\qquad \overline{T}_3=\frac{\overline{f}_3}{\Theta_0}\quad \text{at } x=x_{\text{top}}$$
$$\bar{\sigma}_z(x,z,s)=\overline{P}(s),\qquad \overline{T}_2=\frac{\overline{f}_2}{\Theta_0}\quad \text{at } z=z_{\text{inner}}$$
$$\sigma_x(x,z,t)=0,\qquad \overline{T}_4=\frac{\overline{f}_4}{\Theta_0}\quad \text{at } x=x_{\text{bottom}}$$

and the interface conditions between the kth and $(k+1)$th layers are obtained as

$$(\bar{u}_x,\bar{u}_z,\bar{\sigma}_z,\bar{\tau}_{xz},q,\overline{T})_k=(\bar{u}_x,\bar{u}_z,\bar{\sigma}_z,\bar{\tau}_{xz},q,\overline{T})_{k+1}$$

By applying the boundary conditions and interface conditions to the governing equations, the following equations in matrix form are obtained as

$$[M_1]\{\overline{T}_{ij}\}+[M_2]\{\bar{u}_{zij}\}+[M_3]\{\bar{u}_{xij}\}=0 \tag{37}$$
$$[M_4]\{\overline{T}_{ij}\}+[M_5]\{\bar{u}_{zij}\}+[M_6]\{\bar{u}_{xij}\}=0 \tag{38}$$
$$\big\{[M_7]-s[I]\big\}\{\overline{T}_{ij}\}+s[M_8]\{\bar{u}_{zij}\}+s[M_9]\{\bar{u}_{xij}\}=[M_{10}] \tag{39}$$

Substituting Eqs. (37)–(38) into Eq. (39), yields

$$\big\{[M]-s[I]\big\}\{\overline{T}_{ij}\}=[B][M_{10}] \tag{40}$$

in which

$$[M]=\big\{[M_8][M_2]^{-1}[M_1]+\big([M_8][M_2]^{-1}[M_3]-[M_9]\big)\times\big([M_6]-[M_5][M_2]^{-1}[M_3]\big)^{-1}\times\big([M_5][M_2]^{-1}[M_1]-[M_4]\big)+[I]\big\}^{-1}[M_7]$$

and

$$[B]=\big\{[M_8][M_2]^{-1}[M_1]+\big([M_8][M_2]^{-1}[M_3]-[M_9]\big)\times\big([M_6]-[M_5][M_2]^{-1}[M_3]\big)^{-1}\times\big([M_5][M_2]^{-1}[M_1]-[M_4]\big)+[I]\big\}^{-1}$$

Since the $(N^2\times N^2)$ matrix $[M]$ is a nonsingular real matrix, matrix $[M]$ possesses a set of N^2 linearly independent eigenvectors; hence matrix $[M]$ is diagonalizable. There exists a nonsingular transition matrix $[P]$ such that $[P]^{-1}[M][P]=\text{diag}[M]$, in which the original matrix $[M]$ is similar to the diagonal matrix diag$[M]$, where matrix diag$[M]$ is defined as

$$\text{diag}[M]\begin{bmatrix}\lambda_1 & & & \\ & \lambda_2 & & \\ & & \ddots & \\ & & & \lambda_{N^2}\end{bmatrix} \tag{41}$$

in which λ_j $(j=1,2,\ldots,N^2)$ is the eigenvalue of matrix $[M]$.

By substituting Eq. (41) into (40), the following matrix equation is obtained:

$$\big\{[P]^{-1}[M][P]-s[P]^{-1}[I][P]\big\}[P]^{-1}\{\overline{T}_{ij}\}=[P]^{-1}[B][M_{10}] \tag{42}$$
$$\big\{\text{diag}[M]-s[I]\big\}\big\{\overline{T}^*_{ij}\big\}=[P]^{-1}[B][M_{10}] \tag{43}$$

where

$$\big\{\overline{T}^*_{ij}\big\}=[P]^{-1}\{\overline{T}_{ij}\}$$

The following solution is obtained immediately in the transform domain from Eq. (43).

$$\overline{T}^*_{ij}=\frac{1}{(\lambda_j-s)}[P]^{-1}[B][M_{10}] \tag{44}$$

By taking the inverse Laplace transform on Eq. (44), the solution for $\overline{T}^*_{ij}$ can be obtained. Substituting $\overline{T}^*_{ij}$ into the following relations, the temperature distribution $\overline{T}_{ij}$, the displacements $u_{z_{ij}}$ and $u_{x_{ij}}$ can be obtained as follows:

Table 1
Geometry and material constants of a laminated circular conical shell ($z_{\text{outer}}/z_{\text{inner}} = 1.7$, $L = 4.5$, $\alpha = \pi/6$)

	Layer 1	Layer 2
$E_\eta = E_\theta = E_\zeta$ (N/m^2)	50E6	58E6
$k_\eta = k_\theta = k_\zeta$ (Watt/(m K))	18	22
$\alpha_\eta = \alpha_\theta = \alpha_\zeta$ (1/K)	4E−6	4E−6
$\nu_{\eta\theta} = \nu_{\theta\eta}$	0.2	0.3
$\nu_{\eta\zeta} = \nu_{\zeta\eta}$	0.3	0.2
$\nu_{\zeta\theta} = \nu_{\theta\zeta}$	0.15	0.15
$G_{\eta\zeta}$ (N/m^2)	15E6	18E6
ρ (kg/m^3)	0.095	0.095
C_v (kJ/(kg K))	0.3	0.3
μ (H/m)	1.25E−6	1.1 E−6

$$\{T_{ij}\} = [P]\{T^*_{ij}\} \tag{45}$$

$$\{u_{zij}\} = -[M_2]^{-1}\{[M_1] + [M_3]([M_6] - [M_5][M_2]^{-1}[M_3])^{-1} \times ([M_5][M_2]^{-1}[M_1] - [M_4])\}\{T_{ij}\} \tag{46}$$

$$\{u_{xij}\} = -[M_3]^{-1}[M_1]\{T_{ij}\} - [M_3]^{-1}[M_2]\{u_{zij}\} \tag{47}$$

By substituting T_{ij}, $u_{x_{ij}}$ and $u_{z_{ij}}$ into Eqs. (19)–(22). The x-direction stress σ_x, the circumferential stress σ_θ, z-direction stress σ_z, and the shear stress τ_{xz} can all be obtained.

4. Numerical results and discussions

In this section, some results of the temperature distribution in a laminated circular conical shell, displacement and thermal stresses are calculated numerically. To illustrate the foregoing analysis, numerical calculations for a circular multilayered conical shell subjected to magnetic and vapor fields at the boundary surface were performed. In this examined case, the laminated circular conical shell is composed of two different isotropic layers, in which the nondimensional thickness of each layer is taken for $h_1 = 0.4$ and $h_2 = 0.3$, respectively. The geometrical parameters and the material quantities of this laminated circular conical shell are shown in Table 1. The nondimensional length along the x-direction is $L = 4.5$ and the semi-vertex angle of the cone is $\alpha = \pi/6$. The nondimensional inner and outer radii of the cone at the small and large edges are assumed to be 1.0 and 1.7, respectively. The nondimensional outer and inner temperatures are assumed to be 25 and $f_2(t)$, respectively. The top and bottom nondimensional temperatures are assumed to be 25, respectively. The initial constant magnetic field vector is assumed to be H_0. Furthermore the pressure is assumed to be $p(t)$ on the inner surface.

Table 2
The temperature under different nondimensional times and different number of gird points of finite difference method at $x = 3.13$, $z = 1.33$

	Girds = 36 ($N = 6$)	Girds = 64 ($N = 8$)	Girds = 100 ($N = 10$)	Girds = 144 ($N = 12$)	Girds = 196 ($N = 14$)
$t = 5$	53.112	54.241	54.833	54.951	54.957
$t = 10$	98.965	100.876	101.421	101.483	101.486
$t = 15$	145.113	147.243	147.908	147.993	148.015
$t = 20$	181.832	183.765	184.476	184.542	184.544
$t = 25$	193.324	195.121	195.786	195.856	195.862
$t = 30$	193.896	195.695	196.203	196.230	196.235
$t = 35$	193.985	195.765	196.313	196.319	196.325

For the convergence test of the present method, we calculate the temperature values at the point $x = 3.13$, $z = 1.33$ with different number of finite difference gird points and different time as shown in Table 2. Results show that the temperature changes very small as the number of the grid point increases, say gird points is 144 ($N = 12$). From Table 2, we can see that under various number of gird points of finite difference method, the solutions are rapidly convergent. It is well known that the temperature tends to steady as the time increase. As the time increases, for example, $t = 30$ to 35, the temperatures vary slightly in each layer, since the steady state is approached as the time increases. Therefore, in the present study, we chose gird points = 196 ($N = 14$) to evaluate the temperature distribution,

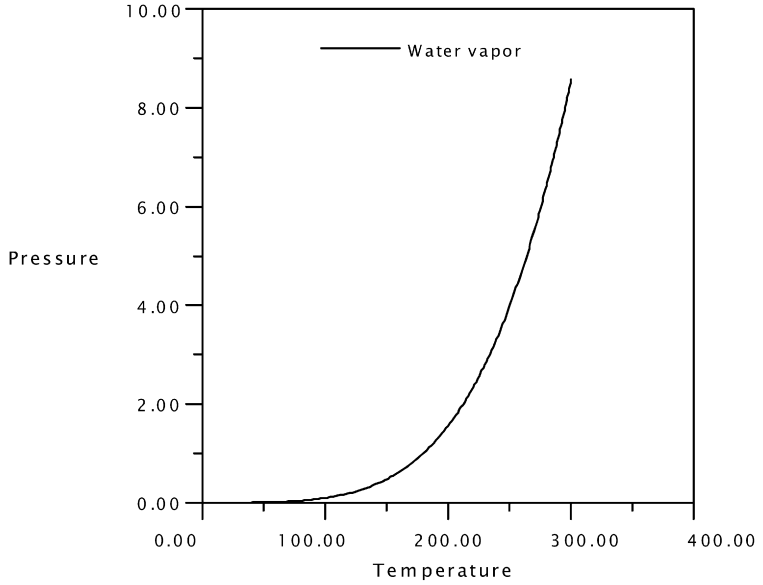

Fig. 2. Temperature and pressure relation in inner boundary (quality 90%) [19].

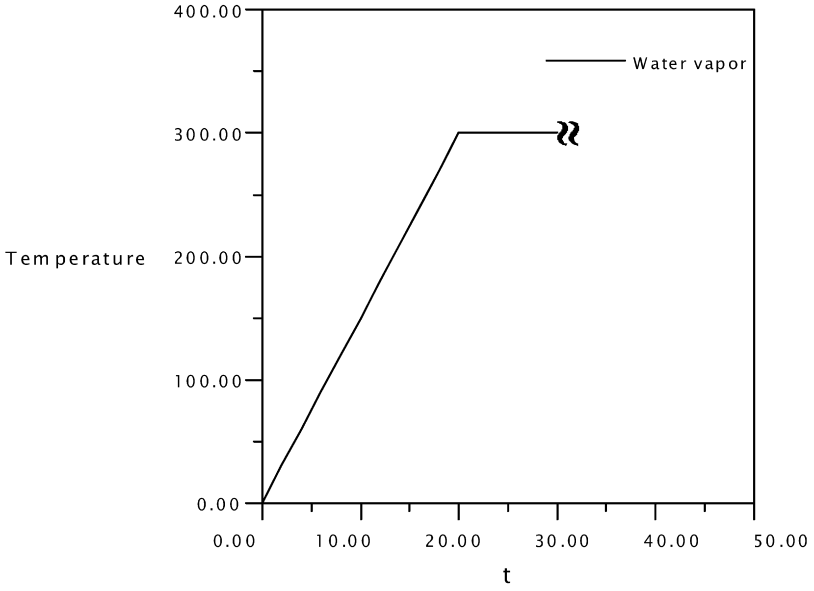

$$f(t)=\begin{cases}15t & , \quad 0\le t\le 20\\ 300 & , \quad t>20\end{cases}$$

Fig. 3. Temperature distribution with time in inner boundary.

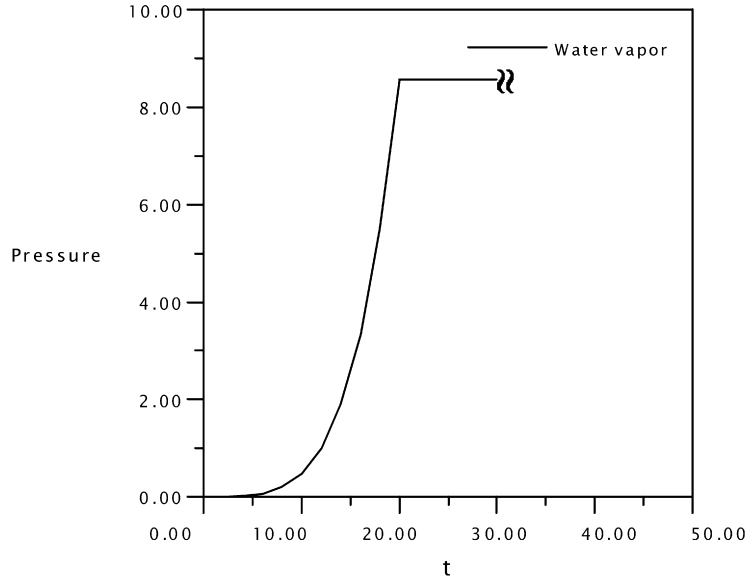

$$p(t)=\begin{cases}-0.00013995t+0.00461523t^2-0.00112473t^3 & \\ +0.00060406t^4 & , \quad 0\le t\le 20\\ 8.585 & , \quad t>20\end{cases}$$

Fig. 4. Pressure distribution with time in inner boundary.

displacement and thermal stresses in a laminated circular conical shell for time $t=10$ and $t=30$.

Fig. 2 shows the water vapor temperature and the pressure relation that are assumed for the inner boundary. The water vapor temperature and pressure data were obtained from a thermodynamic steam table [19]. Fig. 3 shows the temperature distributions with time. Fig. 4 shows the pressure distributions with time. Figs. 5 and 6 show the temperature distribution along the z- and x-direction of the laminated circular conical shell at $t=10$ and 30, respectively. The temperature gradient varies in each layer due to the difference in thermal conductivity coefficients. It is evident that the temperature of boundary surfaces

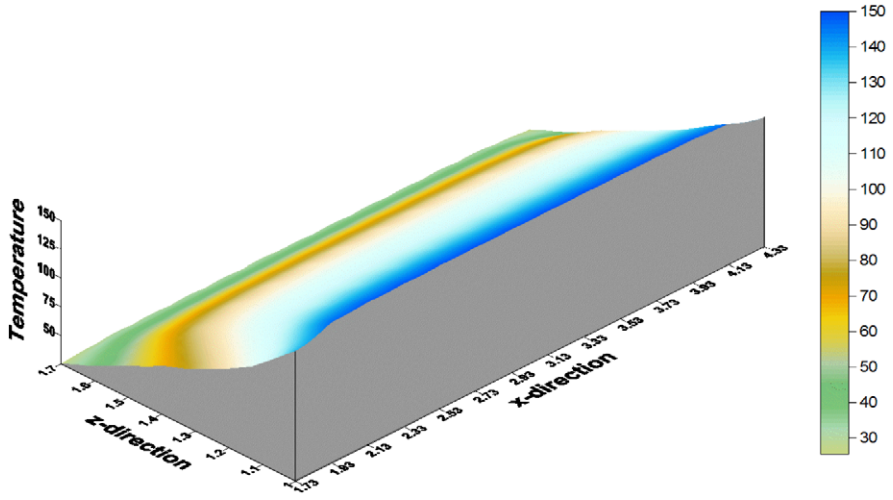

Fig. 5. Temperature distribution along radial and z-directions at $t = 10$.

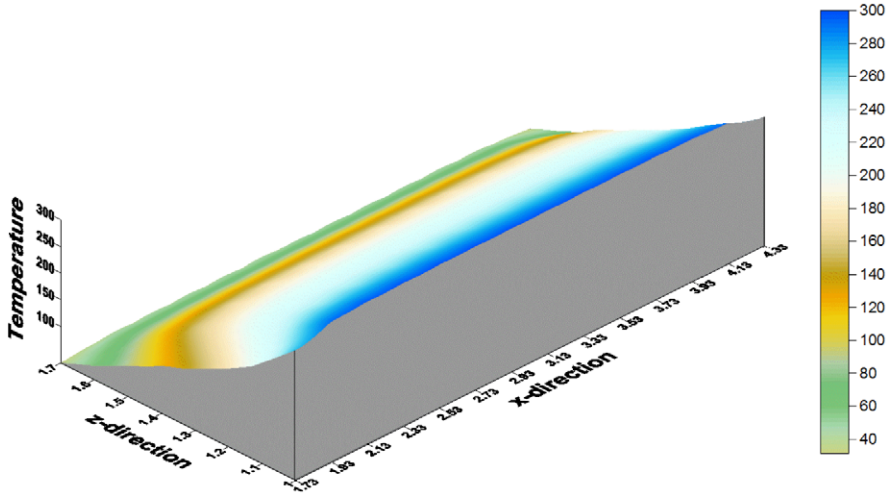

Fig. 6. Temperature distribution along radial and z-directions at $t = 30$.

satisfies the boundary conditions. It can be seen that, the temperature in the outer surface is increasing as the time becomes larger while the laminated circular conical shells are subjected to a time-dependent internal heating process. In both cases, it can be observed that the temperature distribution across each layer is generally curved at time intervals. Fig. 7(a)–(c) shows the variation of displacement in z-direction u_z along the z- and x-directions for the laminated circular conical shell for $H_0 = 0$, 10^6 and 10^7 at $t = 10$, respectively. From these figures, it can be seen that the locations of the points of maximum z-direction displacement along the z-direction occur at the center nearly. It can further be seen that, with the increase of initial constant magnetic field vector, the maximum displacement in z-direction is decreasing. Fig. 8(a)–(c) shows the variation of displacement in z-direction u_z along the z- and x-directions for the laminated circular conical shell for $H_0 = 0$, 10^6 and 10^7 at $t = 30$, respectively. With the increase of the initial constant magnetic field vector, the maximum displacement in z-direction is decreasing. Fig. 9(a)–(c) shows the x-direction displacement varying in the z- and x-directions of the laminated circular conical shells for $H_0 = 0$, 10^6 and 10^7 at $t = 10$, respectively. The locations of the points of maximum x-direction displacement u_x along the z-direction occur at the center. Fig. 10(a)–(c) shows the x-direction displacement varying in the z- and x-directions of the laminated circular conical shells for $H_0 = 0$, 10^6 and 10^7 at $t = 30$, respectively. As the initial constant magnetic field vector increases, we can see the variations of the displacement. Fig. 11(a)–(c) shows the thermal stress distribution σ_z along the z- and x-directions for $H_0 = 0$, 10^6 and 10^7 at $t = 10$, respectively. From these figures, the locations of the points of maximum stress σ_z occur at the inner surfaces (at $z = 1$). Fig. 12(a)–(c) shows the thermal stress distribution σ_z along the z- and x-directions for $H_0 = 0$, 10^6 and 10^7 at $t = 30$, respectively. The z-direction thermal stress changes slightly with respect to initial constant magnetic field vector. Larger the surrounding temperatures will have greater thermal stress σ_z. Fig. 13(a)–(c) shows the circumferential stress σ_θ along the z- and x-directions of the laminated circular conical shell for $H_0 = 0$, 10^6 and 10^7 at $t = 10$, respectively. The locations of the points of maximum stress σ_θ occur at the in-

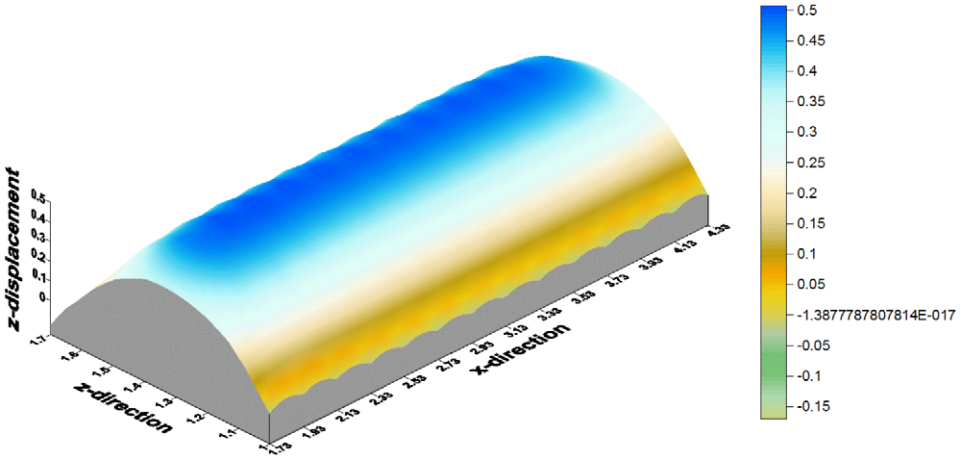

(a)

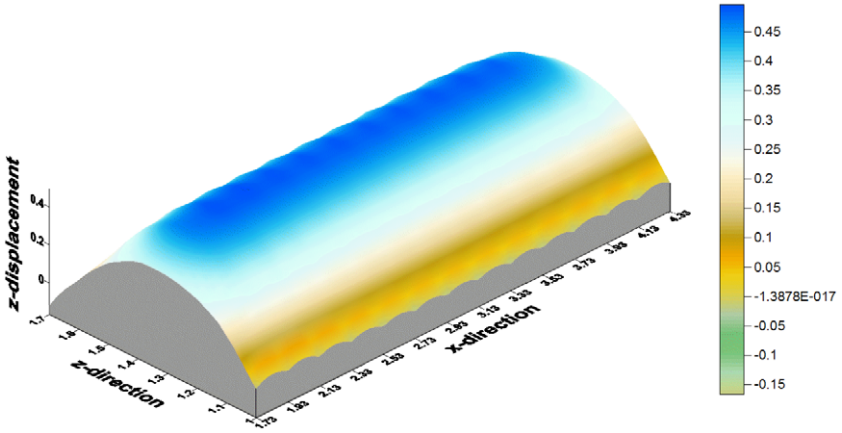

(b)

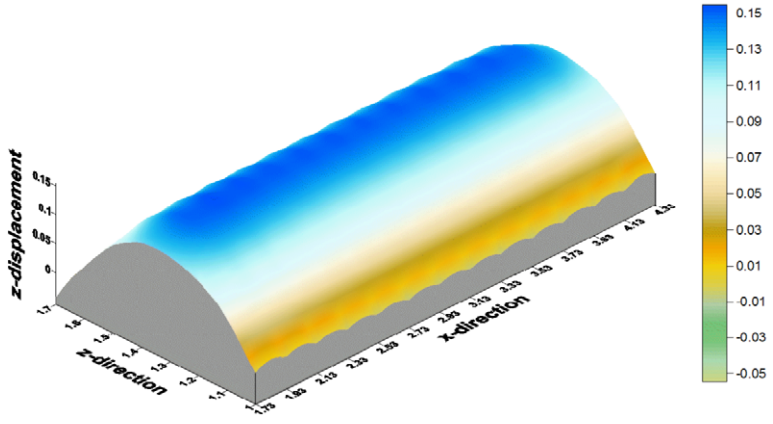

(c)

Fig. 7. Displacement component u_z along z- and x-directions at $t = 10$. (a) $H_0 = 0$, (b) $H_0 = 10^6$, (c) $H_0 = 10^7$.

ner surfaces. Fig. 14(a)–(c) shows the circumferential stress σ_θ along the z- and x-directions of the laminated circular conical shell for $H_0 = 0$, 10^6 and 10^7 at $t = 30$, respectively. The results show that when the initial constant magnetic field vector increases, the circumferential stress distribution changes. Fig. 15(a)–(c) shows the stress distribution σ_x along the z- and x-directions of the laminated circular conical shell for $H_0 = 0$, 10^6 and 10^7 at $t = 10$, respectively. The locations of the points of maximum stress σ_x occur at the inner surfaces. From the figures, it can be noted that the thermal stress distribution σ_z is larger than other thermal stress components because the laminated circular conical shells are subjected to pressure depending on time in the z-direction. Fig. 16(a)–(c) shows the stress distribution σ_x along the z- and x-directions of the laminated circular conical shell for $H_0 = 0$, 10^6 and 10^7 at $t = 30$, respectively. Fig. 17(a)–(c) shows the distributions of the shear stress τ_{xz} in

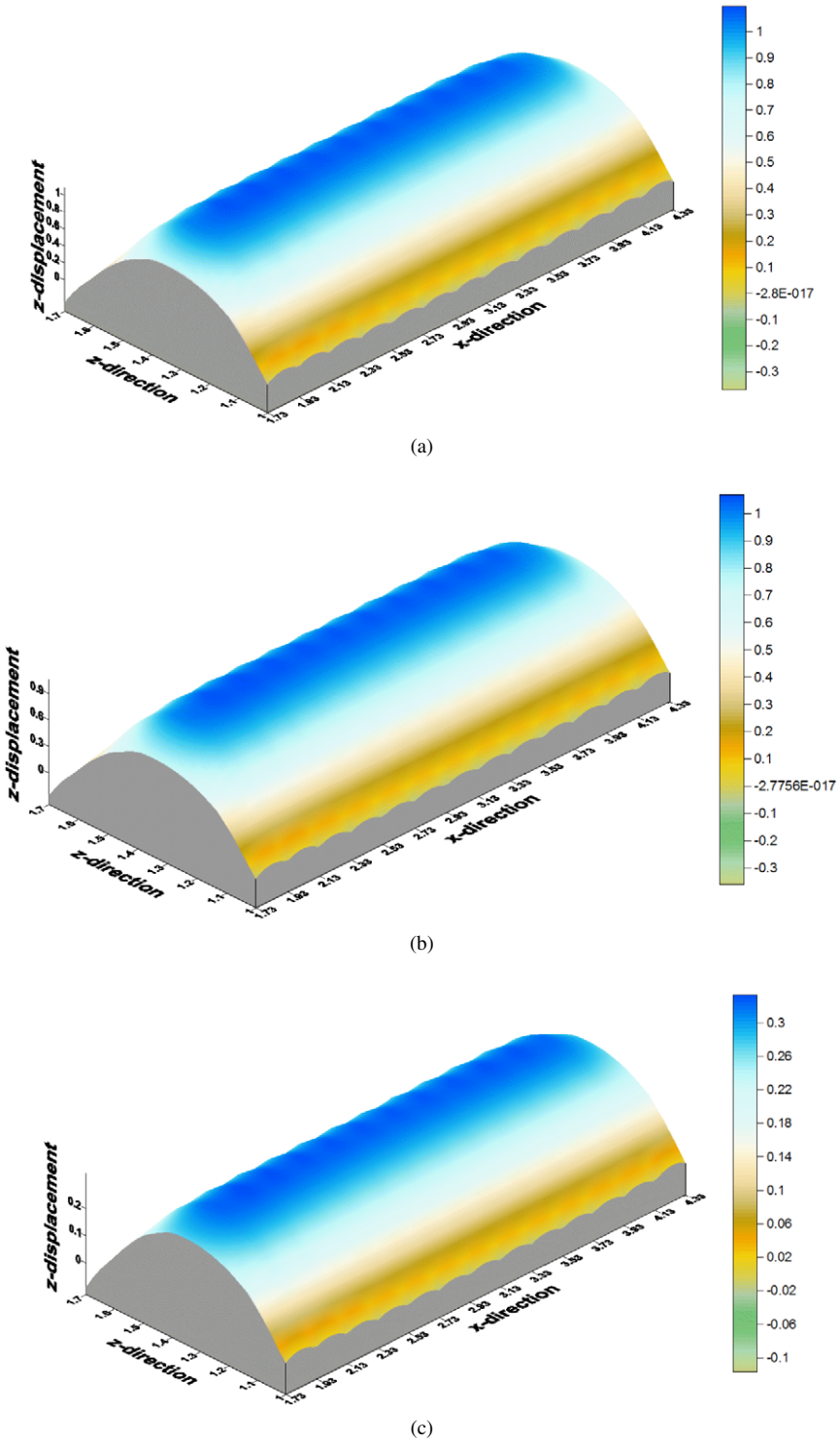

Fig. 8. Displacement component u_z along z- and x-directions at $t = 30$. (a) $H_0 = 0$, (b) $H_0 = 10^6$, (c) $H_0 = 10^7$.

the laminated circular conical shell at $t = 10$ for $H_0 = 0$, 10^6 and 10^7, respectively. Fig. 18(a)–(c) shows that the distribution of the shear stress τ_{xz} in the laminated circular conical shell at $t = 30$ for $H_0 = 0$, 10^6 and 10^7, respectively. The shear stress changes slightly with respect to initial constant magnetic field vector. The shear stress τ_{xz} is much smaller than the other thermal stress components.

The above discussions demonstrate that the present method for the conical coordinates can obtain stable solutions at a specific time. Thus it is a powerful and efficient method for solving the coupled transient magnetothermoelastic problems of a circular multilayered conical shell. These results are specific for the boundary conditions considered, and other assumptive boundary conditions may have different trends.

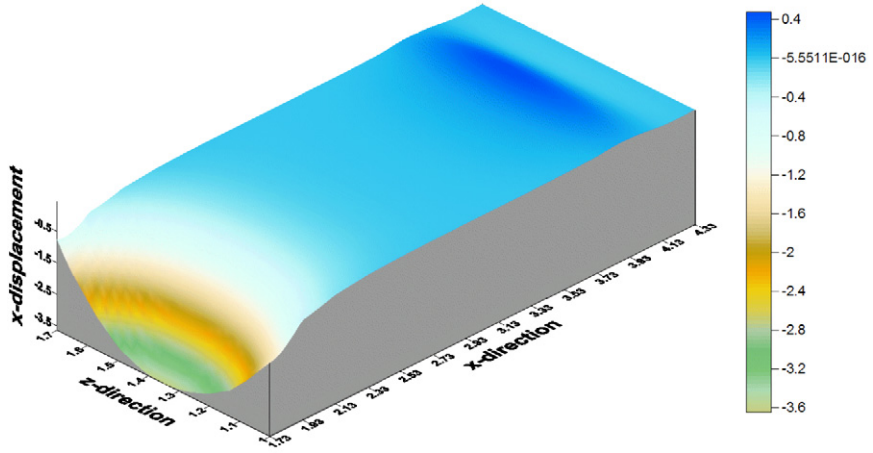

(a)

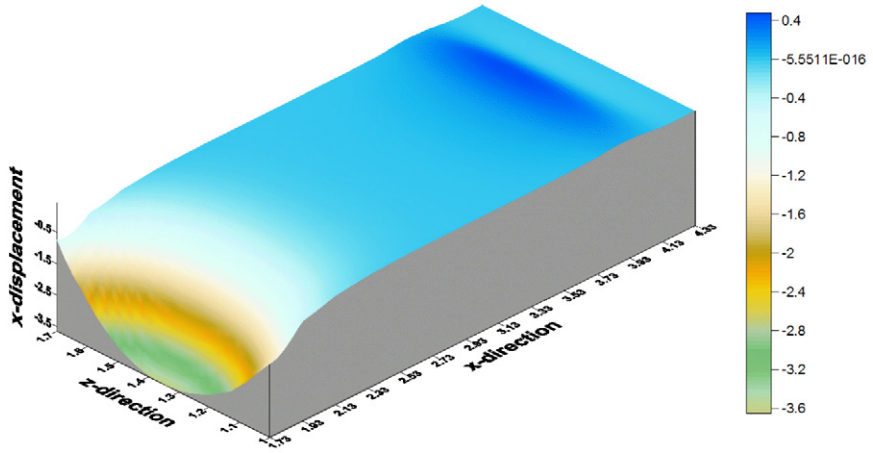

(b)

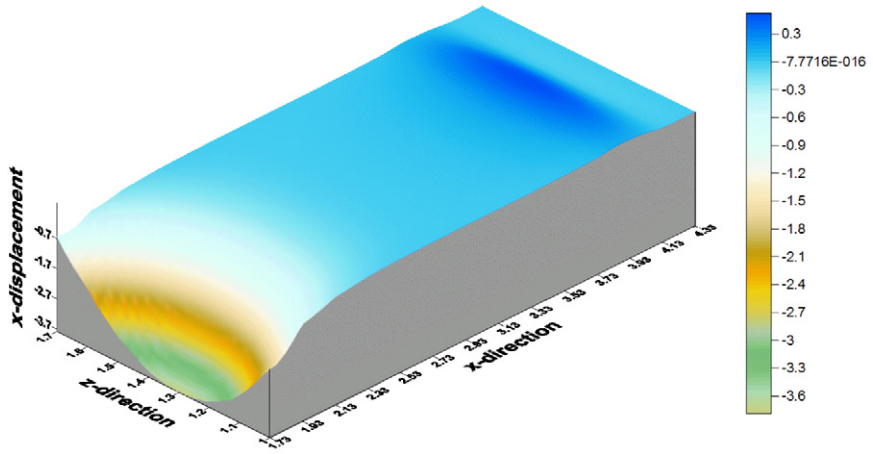

(c)

Fig. 9. Displacement component u_x along z- and x-directions at $t = 10$. (a) $H_0 = 0$, (b) $H_0 = 10^6$, (c) $H_0 = 10^7$.

5. Conclusions

In this paper, the magnetothermoelastic transient response of the laminated circular conical shell has been analyzed. The magnetothermoelastic problem of circular conical shell composed of multilayer of different materials and subjected to magnetic and vapor fields have also been discussed. It was shown that the solutions are rapidly convergent. Solutions for the temperature, displacement and thermal stress distributions in both transient and steady state are obtained. The present method can obtain stable solutions at a specific time; thus it is a further concluded that the method and the computing process of the

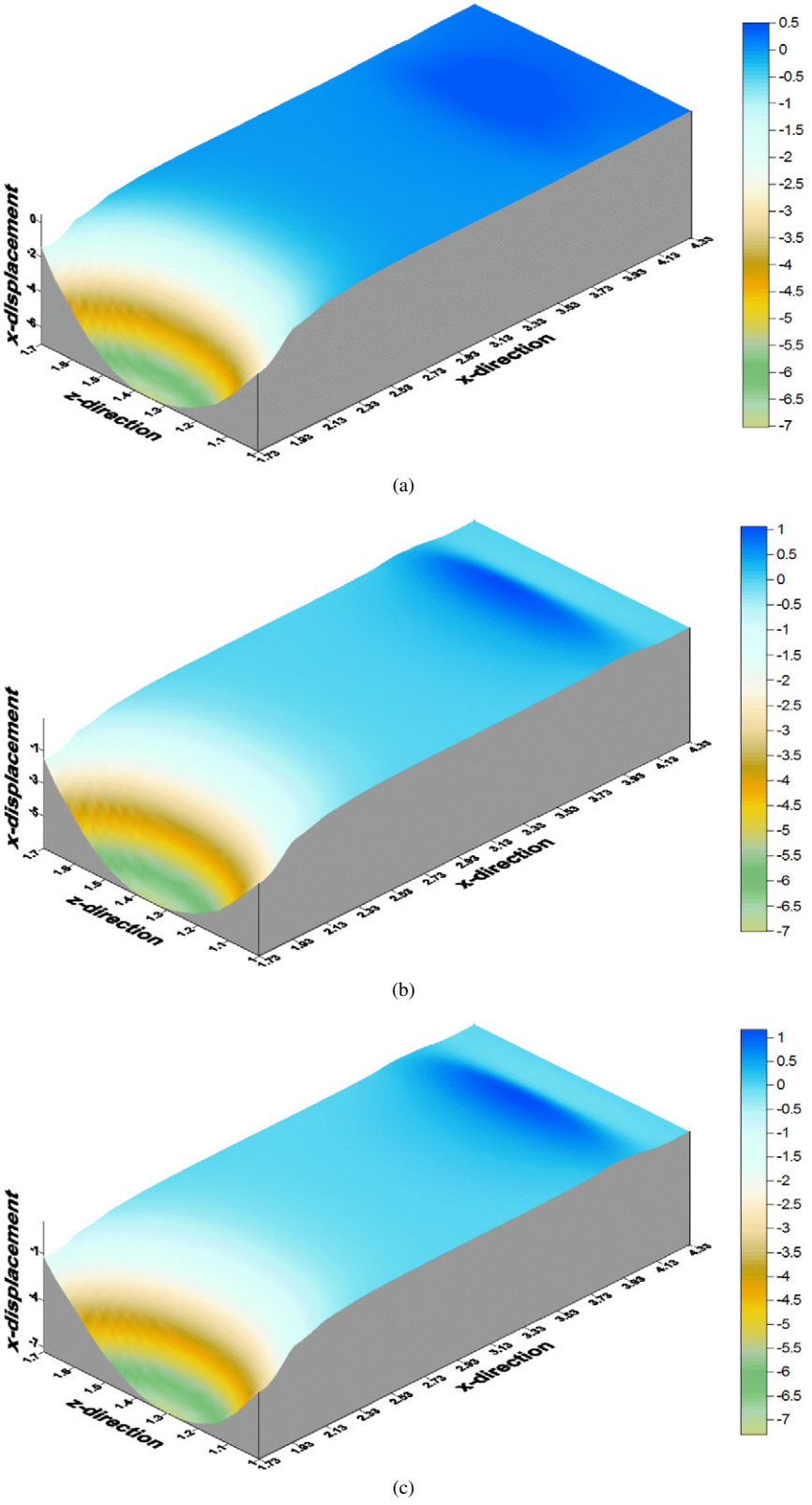

Fig. 10. Displacement component u_x along z- and x-directions at $t = 30$. (a) $H_0 = 0$, (b) $H_0 = 10^6$, (c) $H_0 = 10^7$.

coupled transient magnetothermoelastic problems of a circular multilayered conical shell are powerful and efficient. The topic studied here is relevant to many potential applications in space shuttles, supersonic airplanes, rockets and missiles, plasma physics and the corresponding measurement techniques of magnetothermoelasticity. This paper is well organized and presented clearly, with understandable technical derivation and very meaningful numerical results.

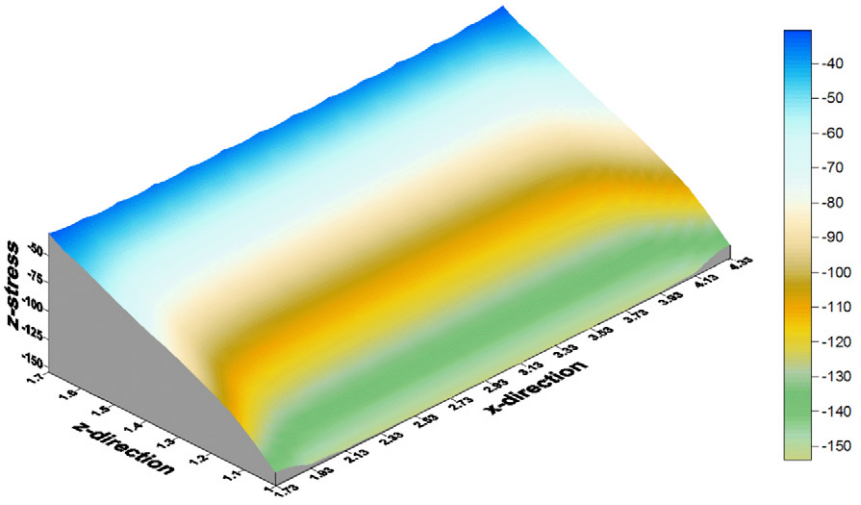

(a)

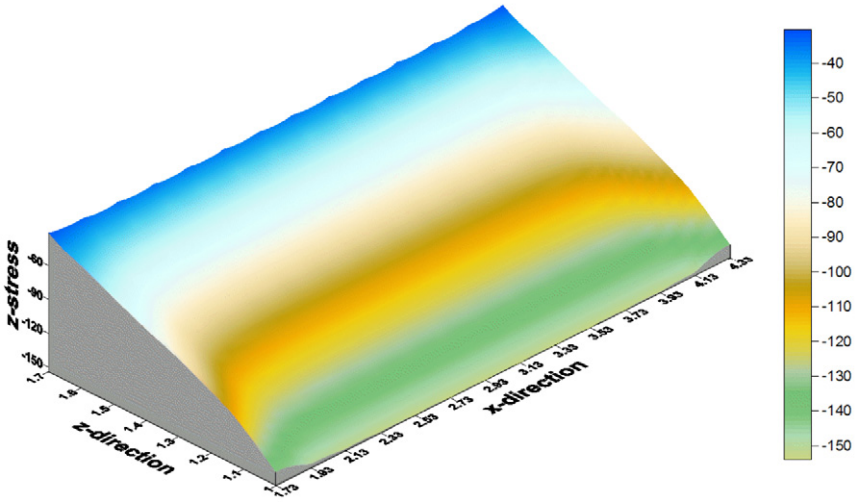

(b)

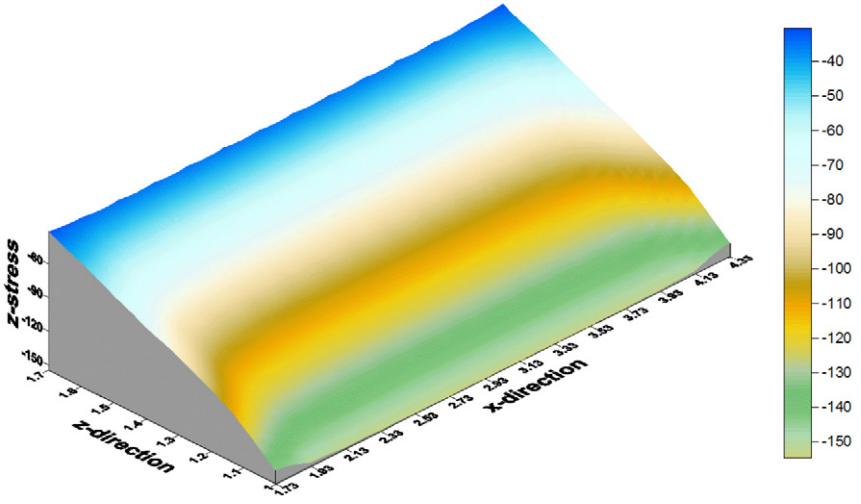

(c)

Fig. 11. Stress distribution σ_z along z- and x-directions at $t = 10$. (a) $H_0 = 0$, (b) $H_0 = 10^6$, (c) $H_0 = 10^7$.

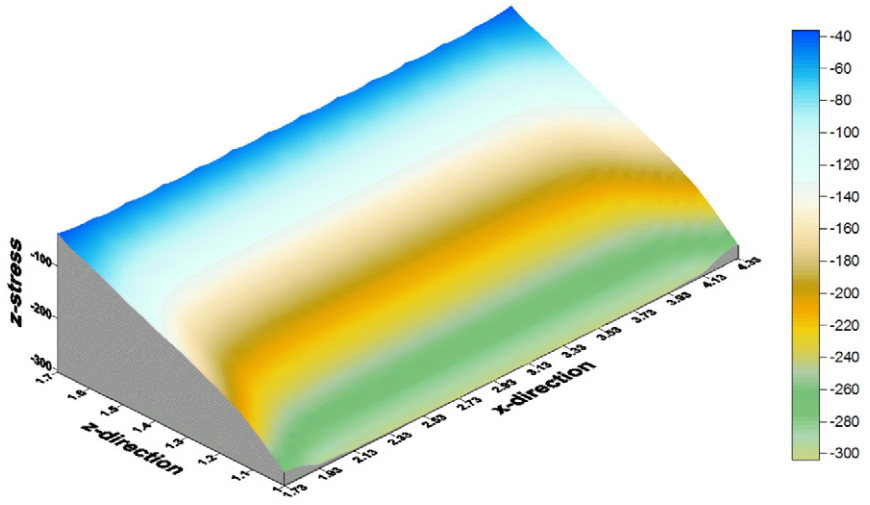

(a)

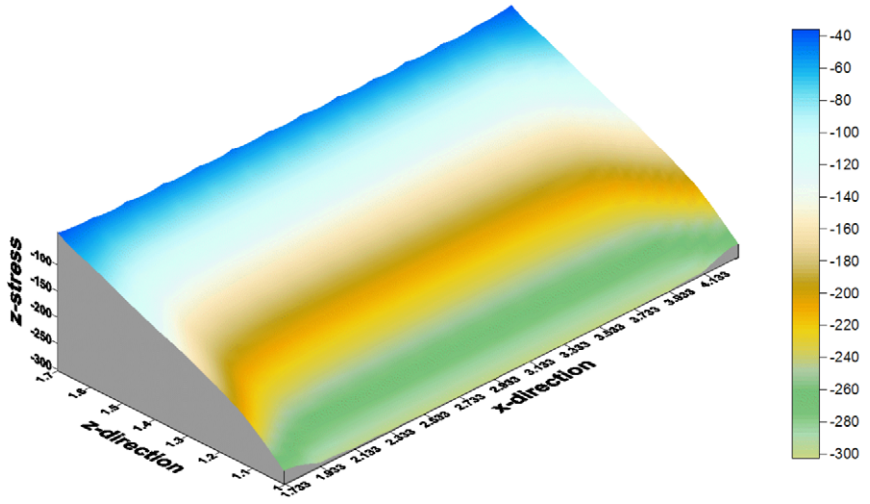

(b)

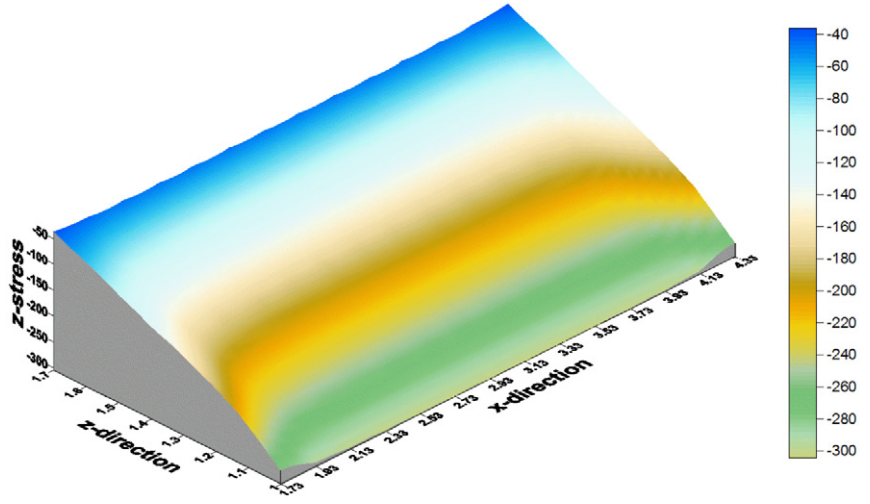

(c)

Fig. 12. Stress distribution σ_z along z- and x-directions at $t = 30$. (a) $H_0 = 0$, (b) $H_0 = 10^6$, (c) $H_0 = 10^7$.

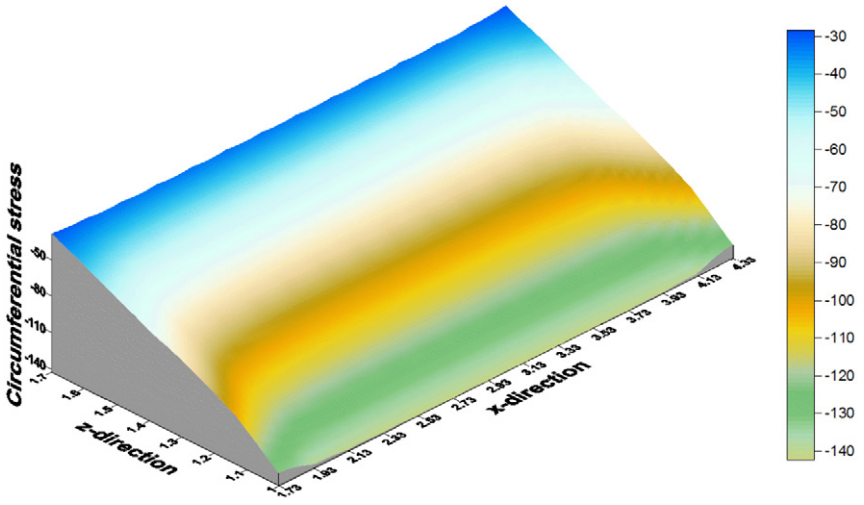

(a)

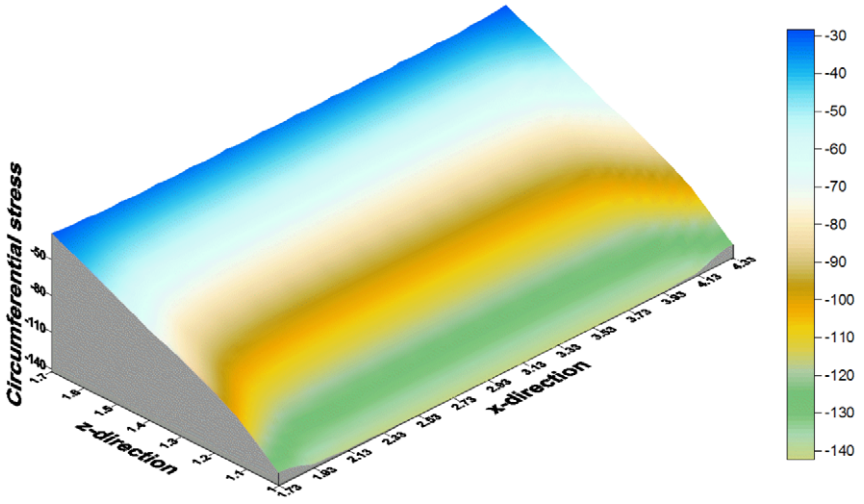

(b)

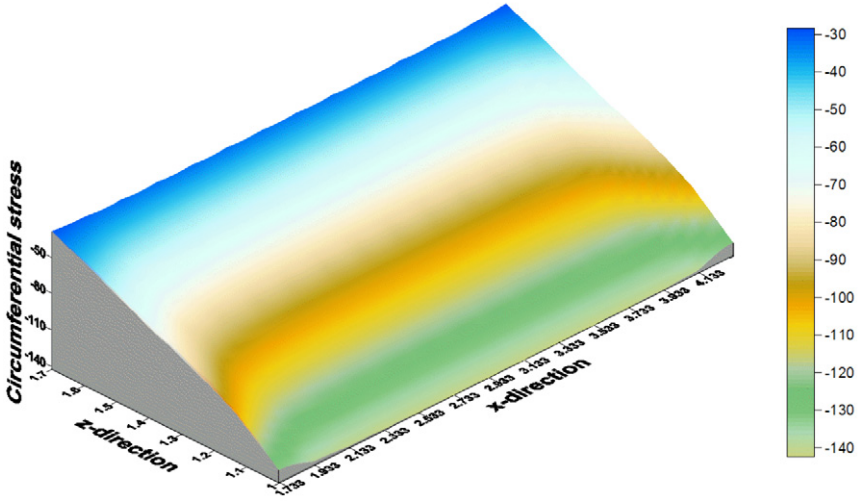

(c)

Fig. 13. Circumferential stress along z- and x-directions at $t = 10$. (a) $H_0 = 0$, (b) $H_0 = 10^6$, (c) $H_0 = 10^7$.

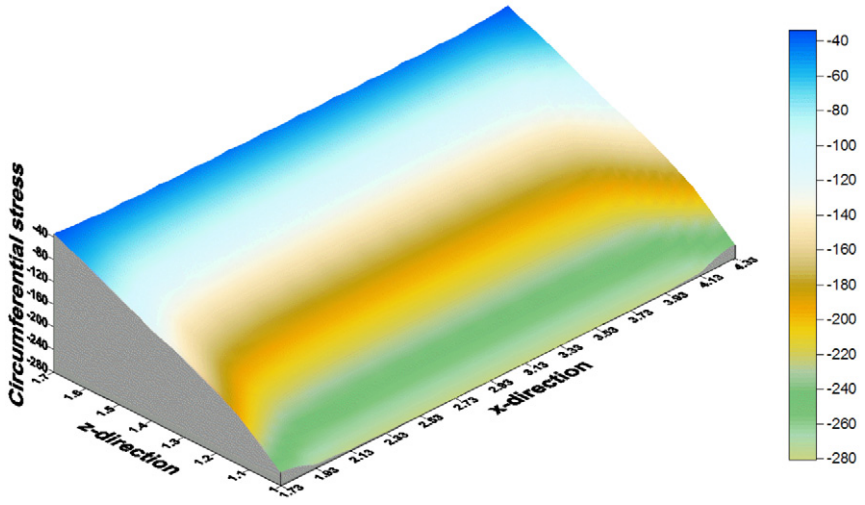

(a)

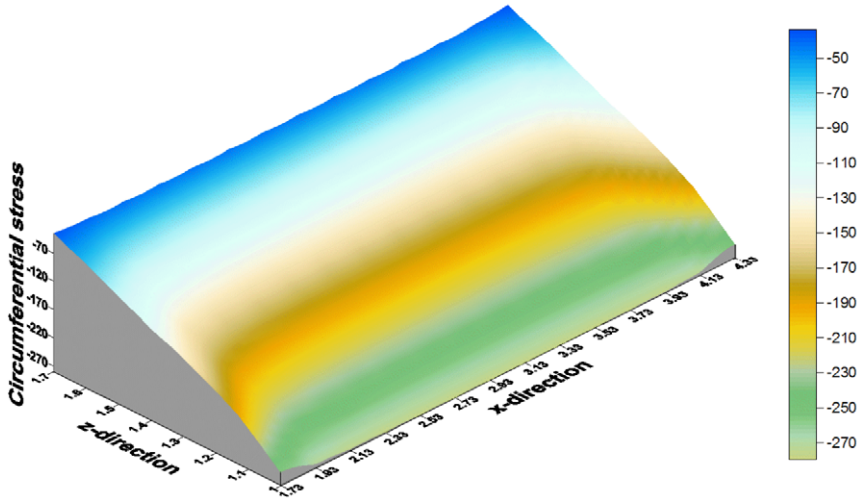

(b)

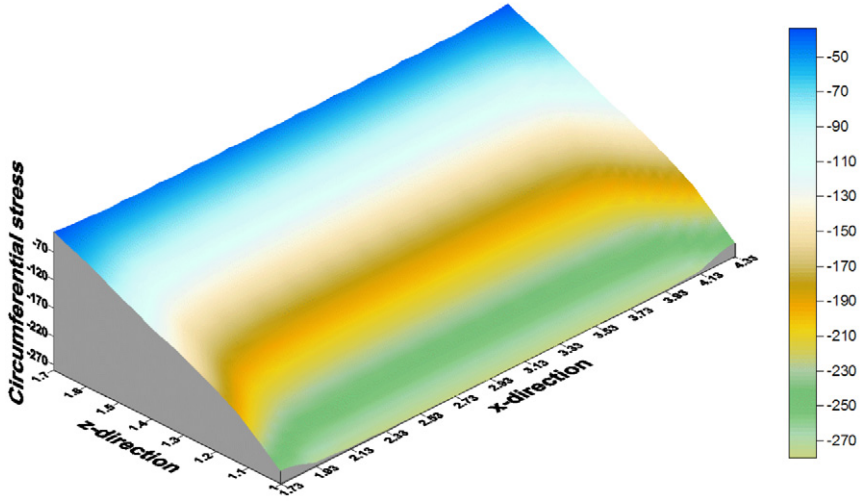

(c)

Fig. 14. Circumferential stress along z- and x-directions at $t = 30$. (a) $H_0 = 0$, (b) $H_0 = 10^6$, (c) $H_0 = 10^7$.

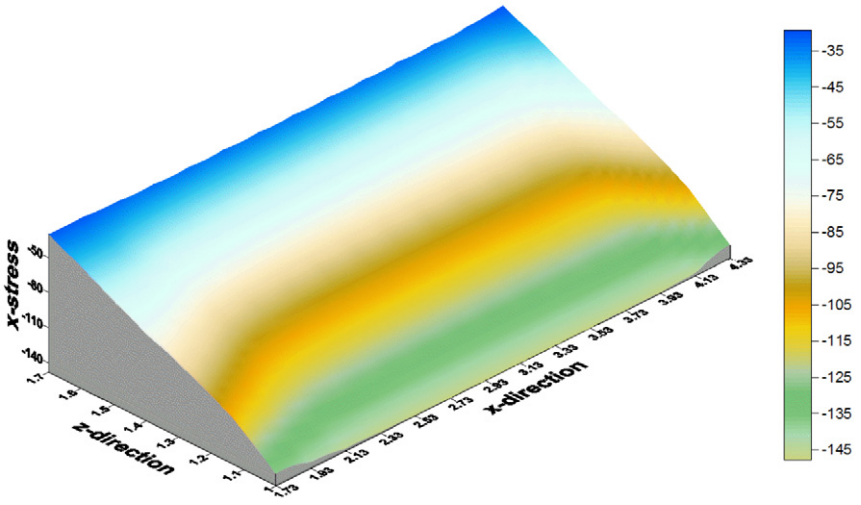

(a)

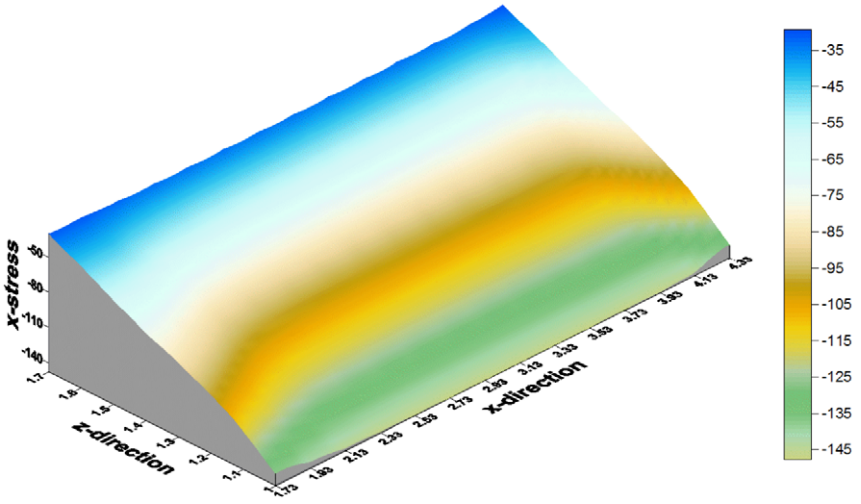

(b)

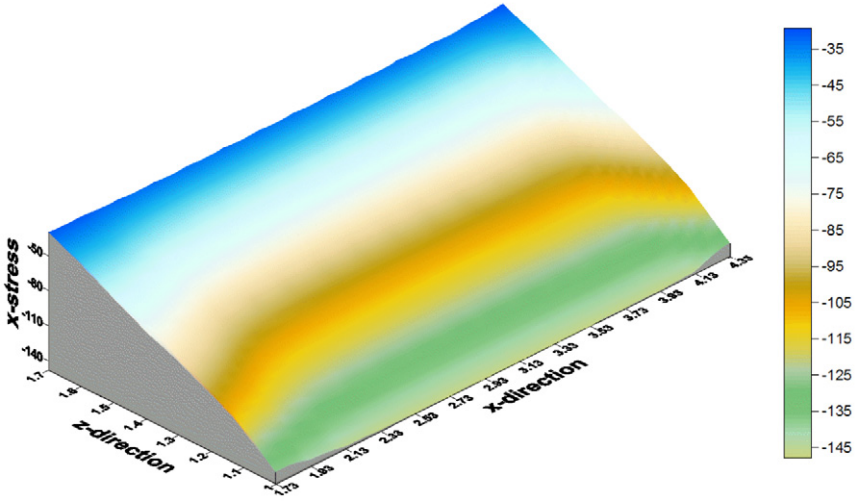

(c)

Fig. 15. Stress distribution σ_x along z- and x-directions at $t = 10$. (a) $H_0 = 0$, (b) $H_0 = 10^6$, (c) $H_0 = 10^7$.

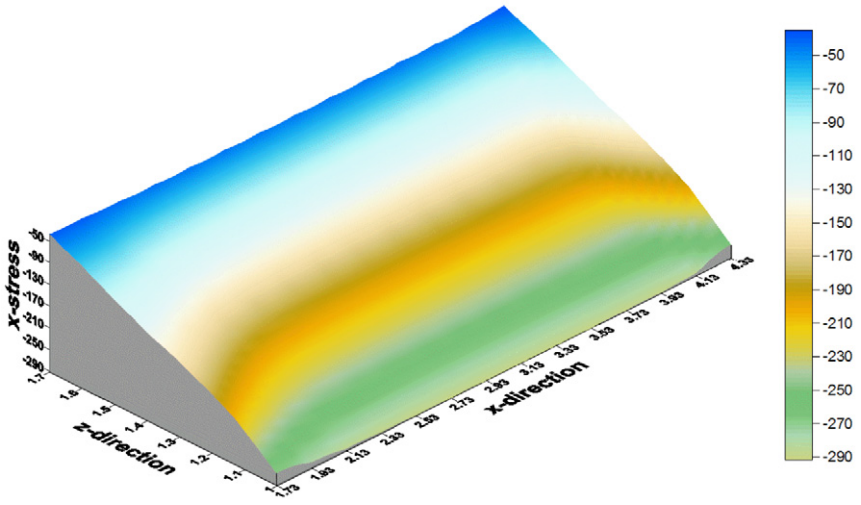

(a)

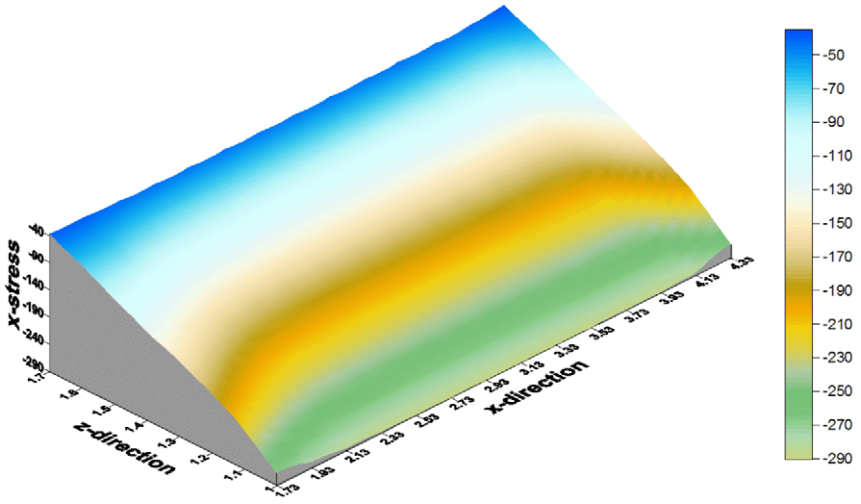

(b)

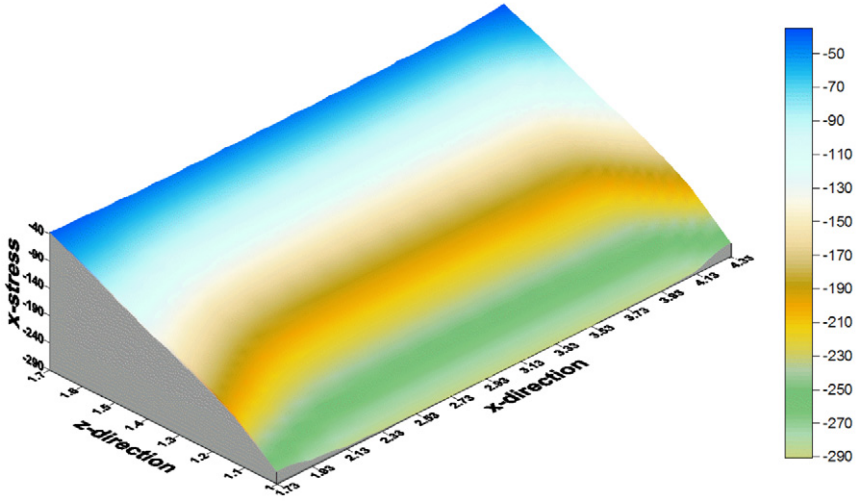

(c)

Fig. 16. Stress distribution σ_x along z- and x-directions at $t = 30$. (a) $H_0 = 0$, (b) $H_0 = 10^6$, (c) $H_0 = 10^7$.

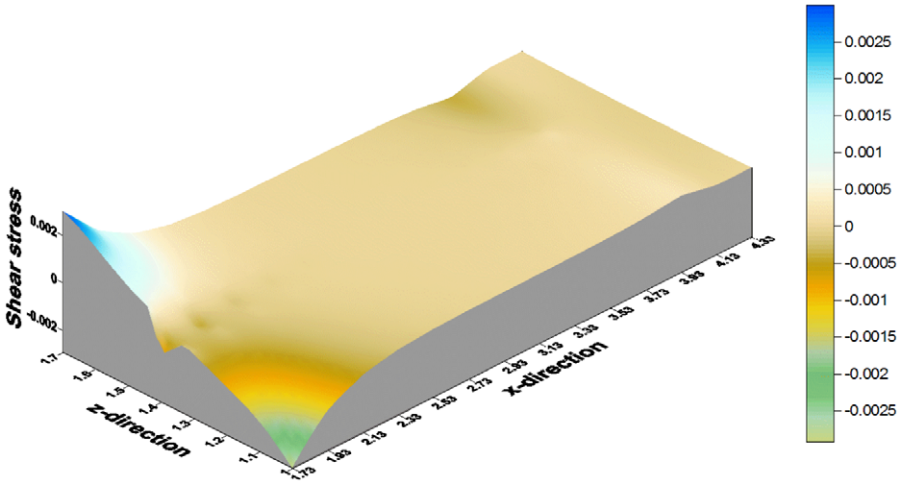

(a)

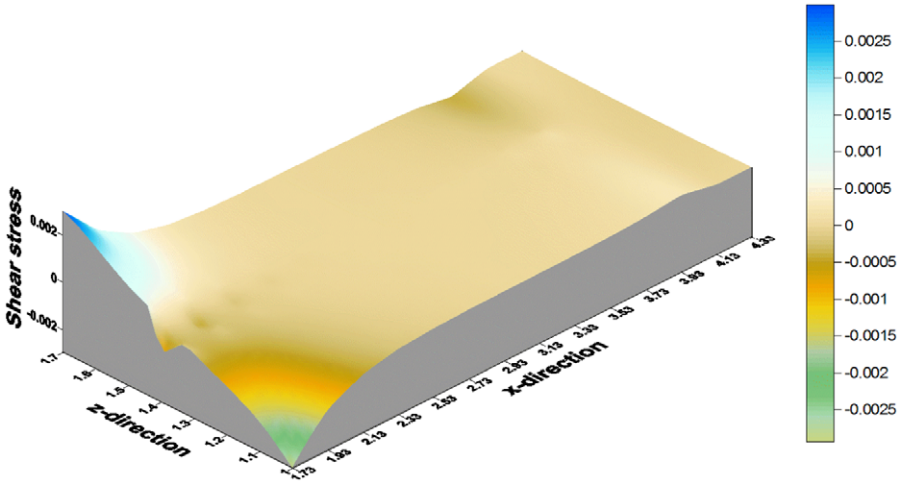

(b)

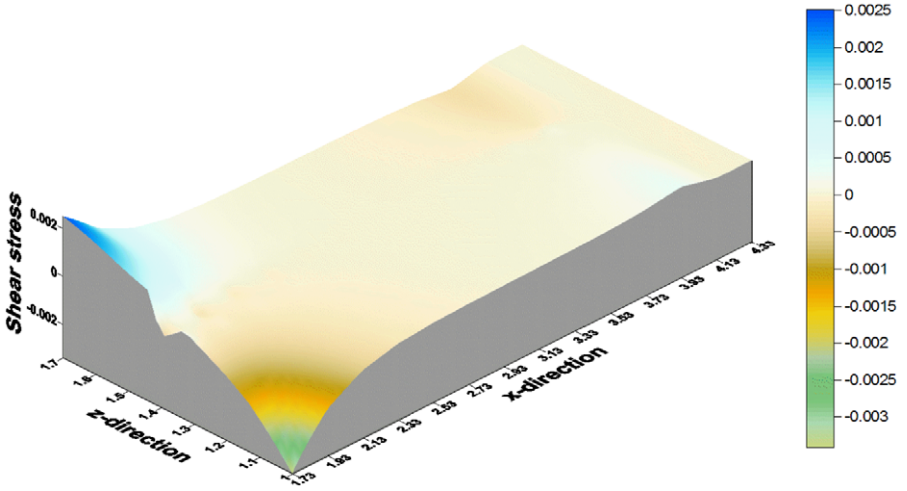

(c)

Fig. 17. Shear stress distribution τ_{xz} along z- and x-directions at $t = 10$. (a) $H_0 = 0$, (b) $H_0 = 10^6$, (c) $H_0 = 10^7$.

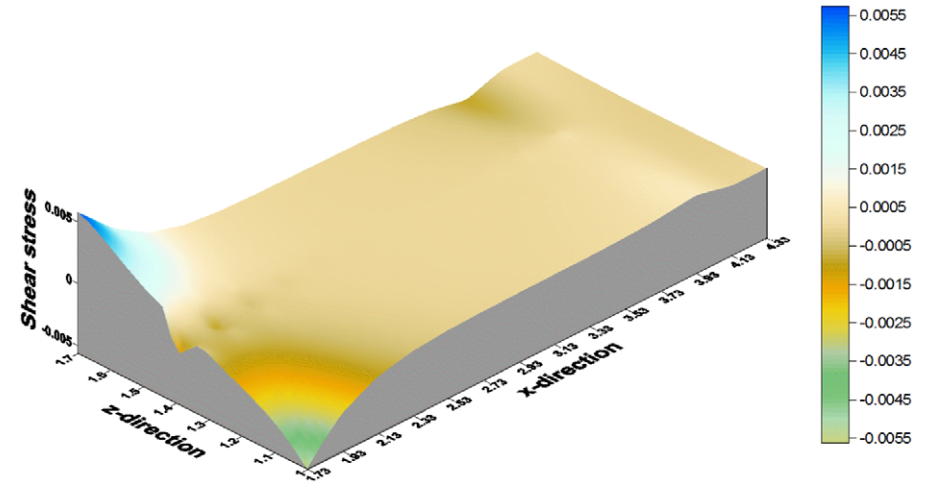

(a)

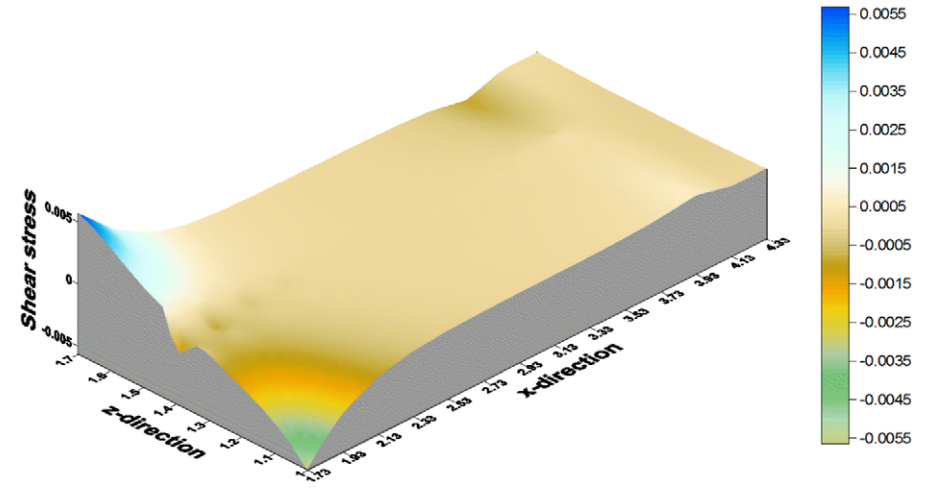

(b)

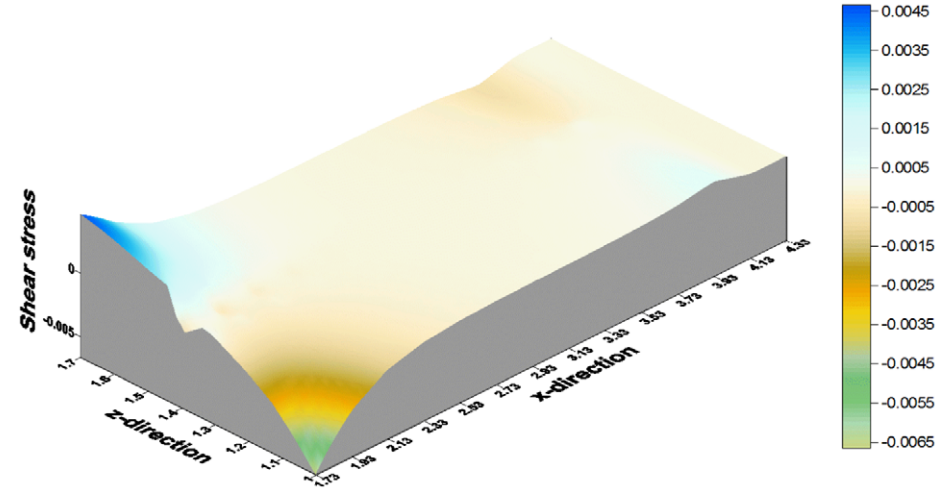

(c)

Fig. 18. Shear stress distribution τ_{xz} along z- and x-directions at $t = 30$. (a) $H_0 = 0$, (b) $H_0 = 10^6$, (c) $H_0 = 10^7$.

Acknowledgement

The authors are thankful to the National Science Council of the Republic of China for supporting this research under grant NSC-96-2221-E-164-007.

References

[1] N.S. Al-Huniti, M.A. Al-Nimr, Thermoelastic response of a heated thin composite plate using the hyperbolic heat conduction model: lumped analysis, International Journal of Thermal Sciences 43 (10) (2004) 959–965.

[2] P. Hosseini-Tehrani, A.R. Hosseini-Godarzi, Dynamic crack analysis under thermal shock considering Lord–Shulman theory, International Journal of Thermal Sciences 43 (10) (2004) 1003–1010.

[3] P. Ram, N. Sharma, R. Kumar, Thermomechanical response of generalized thermoelastic diffusion with one relaxation time due to time harmonic sources, International Journal of Thermal Sciences 47 (3) (2008) 315–323.

[4] H.L. Dai, X. Wang, Stress wave propagation in laminated piezoelectric spherical shells under thermal shock and excitation, European Journal of Mechanics A/Solids 24 (2005) 263–276.

[5] X. Wang, G. Lu, S.R. Guillow, Stress wave propagation in orthotropic laminated thick-walled spherical shells, International Journal of Solids and Structures 39 (15) (2002) 4027–4037.

[6] X. Wang, K. Dong, Magnetothermodynamic stress and perturbation of magnetic field vector in a non-homogeneous thermoelastic cylinder, European Journal of Mechanics A/Solids 25 (2006) 98–109.

[7] X. Wang, H.L. Dai, Magnetothermodynamic stress and perturbation of magnetic field vector in an orthotropic thermoelastic cylinder, International Journal of Engineering Science 42 (2004) 539–556.

[8] H.L. Dai, X. Wang, Magnetoelastodynamic stress and perturbation of magnetic field vector in an orthotropic laminated hollow cylinder, International Journal of Engineering Science 44 (5–6) (2006) 365–378.

[9] P. Jianpong, I.E. Harik, Iterative FD solution to bending of axi-symmetric conical shells, Journal of Structural Engineering 116 (1990) 2433–2446.

[10] C.H. Lu, R. Mao, D.C. Winfield, Stress analysis of thick laminated conical tubes with variable thickness, Composites Engineering 5 (1995) 471–484.

[11] C.P. Wu, S.J. Chiu, Thermally induced dynamic instability of laminated composite conical shells, International Journal of Solids and Structures 39 (2002) 3001–3021.

[12] C.P. Wu, S.J. Chiu, Thermoelastic buckling of laminated composite conical shells, Journal of Thermal Stresses 24 (2001) 881–901.

[13] C.K. Chen, H.T. Chen, Application of hybrid Laplace transform finite-different method to transient heat conduction problem, Numerical Heat Transfer 14 (3) (1988) 343–356.

[14] C.K. Chen, H.T. Chen, T.M. Chen, Hybrid Laplace transform finite-element method for one-dimensional transient heat conduction problems, Comp. Methods Appl. Mech. Eng. 63 (1987) 83–95.

[15] K.C. Jane, Z.Y. Lee, Thermoelastic transient response of an infinitely long multilayered cylinder, Mechanics Research Communication 26 (6) (1999) 709–718.

[16] C.K. Chen, C.I. Hung, Z.Y. Lee, Transient thermal stresses analysis of multilayered hollow cylinder, ACTA Mechanica 151 (2001) 75–88.

[17] Z.Y. Lee, C.K. Chen, C.I. Hung, Thermoelastic transient response of multilayered hollow cylinder with initial interface pressure, Journal of Thermal Stresses 24 (2001) 987–1006.

[18] K. John, Electromagnetics, McGraw-Hill, Inc., New York, 1984.

[19] G.V. Wylen, R. Sanntag, C. Borgnakke, Fundamentals of Classical Thermodynamics, John Wiley & Sons, New York, 1994.